Automobile demand forecasting: Spatiotemporal and hierarchical modeling, life cycle dynamics, and user-generated online information

Tom Nahrendorf^{a,b}, Stefan Minner^{a,c}, Helfried Binder^b, Richard Zinck^b

^aSchool of Management, Technical University of Munich, Arcisstraße 21, Munich, 80333, Bavaria, Germany
 ^bBMW AG, Petuelring 130, Munich, 80809, Bavaria, Germany
 ^cMunich Data Science Institute, Walther-von-Dyck-Straße 10, Garching, 85748, Bavaria, Germany

Abstract

Premium automotive manufacturers face increasingly complex forecasting challenges due to high product variety, sparse variant-level data, and volatile market dynamics. This study addresses monthly automobile demand forecasting across a multi-product, multi-market, and multi-level hierarchy using data from a German premium manufacturer. The methodology combines point and probabilistic forecasts across strategic and operational planning levels, leveraging ensembles of LightGBM models with pooled training sets, quantile regression, and a mixed-integer linear programming reconciliation approach. Results highlight that spatiotemporal dependencies, as well as rounding bias, significantly affect forecast accuracy, underscoring the importance of integer forecasts for operational feasibility. Shapley analysis shows that short-term demand is reactive, shaped by life cycle maturity, autoregressive momentum, and operational signals, whereas medium-term demand reflects anticipatory drivers such as online engagement, planning targets, and competitive indicators, with online behavioral data considerably improving accuracy at disaggregated levels. Keywords: Machine learning, Multivariate time series, Leading indicators, Forecasting practice, Automotive industry

1. Introduction

Premium original equipment manufacturers (OEMs) pursue mass customization strategies, offering substantially greater product variety than volume manufacturers. On average, German premium OEMs provide more than five times as many factory-fitted options as their Japanese volume-brand

counterparts (Staeblein & Aoki, 2015). Such strategies lead to increasingly diverse product portfolios, resulting in greater demand fragmentation, increasing uncertainty at the individual product level, and higher costs associated with supply–demand mismatches (Moreno & Terwiesch, 2016). Consequently, the forecasting problem for premium OEMs extends beyond aggregate product-level demand to a large number of low-volume variants, referred to as product types hereafter. The combination of high dimensionality and sparse historical data for many configurations further amplifies forecast uncertainty and poses substantial challenges for supply chain planning.

Automobile demand forecasts play a central role in supporting both strategic and operational decision-making. Key applications include production and capacity planning, pricing, inventory management, and marketing. These decisions span different organizational levels and time horizons, requiring forecasts across multiple levels of the product and market hierarchy, from aggregated brands and regions to specific product types. While high-level forecasts inform long-term strategic planning, lower-level forecasts are critical for short- to medium-term operational decisions. The value of improved forecasting lies not only in higher predictive accuracy, but also in more effective decision-making through reduced operational costs, more efficient resource allocation, and better risk management. In particular, probabilistic forecasts are essential for risk-aware decision-making, as they quantify forecast uncertainty, which is crucial for applications such as pricing, capacity buffering, and inventory control. Quantile regression has thus gained attention as a means of modeling the full distribution of demand, rather than relying solely on point forecasts.

Despite its importance, automotive demand forecasting presents several distinctive and underexplored challenges. First, strict product hierarchies require coherent forecasts across multiple levels. Forecasting models should explicitly ensure this structural consistency. Second, demand patterns are shaped by complex life cycle dynamics: five- to seven-year product cycles, mid-cycle facelifts, and overlapping launches generate irregular, multi-peak demand curves that are difficult to capture with standard life cycle models. Third, spatiotemporal correlations across geographic regions and over time significantly influence demand, yet remain difficult to model effectively. Finally, the increasing digitalization of the automotive sales process enables demand sensing through usergenerated data, such as online configurator website traffic, although their predictive value remains unclear in the forecasting literature (Schaer et al., 2019).

While hierarchical forecasting, life cycle dynamics, spatiotemporal dependencies, and behavioral

data have each been studied independently, they have not been jointly addressed within a real-world automotive forecasting framework. To fill this gap, we present an empirical study conducted in collaboration with a German premium OEM and investigate the following research questions: (RQ1) Which point and probabilistic forecasting methods yield the highest accuracy in predicting automobile demand at various hierarchical levels? (RQ2) What are the key spatiotemporal, endogenous, and exogenous factors influencing automobile demand? (RQ3) To what extent does user-generated online information improve forecast accuracy?

To answer these questions, we apply light gradient boosting machine learning (LightGBM; Ke et al., 2017) models with quantile regression to estimate the full distribution of demand, extending the global architecture used in the M5 competitions (Makridakis et al., 2022a,b). Building on this foundation, we introduce a probabilistic pooled ensemble (direct-recursive averaging) and replace fixed hierarchical pooling with data-driven pooling-set selection that trades off accuracy and complexity. To address the variant-level forecasting challenges of premium OEMs, we propose a mixed-integer linear programming (MILP) integer-coherent reconciliation method. This ensures coherent forecasts across the hierarchy while preserving integer demand values, avoiding rounding errors that can distort manufacturing and supply chain operations. We further employ explainable artificial intelligence (XAI) to identify influential demand drivers (RQ2) and evaluate the contribution of user-generated online information through statistical testing (RQ3).

The remainder of the paper is structured as follows: Section 2 reviews related work and theoretical foundations. Section 3 presents the modeling, forecasting, and data pooling strategies employed, along with our proposed reconciliation approach. Section 4 describes the empirical case study, including the data characteristics and the forecast evaluation metrics. Section 5 reports the results addressing RQ1–RQ3. Finally, Section 6 concludes the paper and outlines directions for future research.

2. Related literature

2.1. Automotive demand forecasting and probabilistic methods

Prior research in the automotive domain has predominantly addressed macroeconomic modeling of total vehicle sales (e.g., Berkovec, 1985), using dynamic simulation frameworks to study aggregate demand patterns. More recent work has targeted brand-level (e.g., Fantazzini & Toktamysova,

2015) or component-level forecasts, such as spare parts and batteries (e.g., Bottani et al., 2021; Gonçalves et al., 2021), employing machine learning (ML) approaches. These studies have relied on aggregated data and point forecasts. However, high-granularity demand forecasting at the market-product type level remains underexplored, particularly for premium OEMs and in settings that require quantification of forecast uncertainty.

Quantile regression methods have gained traction for their ability to estimate full conditional distributions rather than single-point estimates. Recent studies demonstrate the effectiveness of tree-based quantile models across various domains: Arora et al. (2023) applied quantile regression forests (QRF) to predict patient waiting times in emergency departments, which led to a more uniform patient load across the network. Guo et al. (2021) used regression trees to forecast airport transfer times, leading to reduced staffing costs, while Salari et al. (2022) showed that cost-sensitive QRFs improved customer satisfaction and boosted e-commerce sales through better delivery time prediction. The value of quantile-based forecasting has also been confirmed in recent forecasting competitions. In the M5 Uncertainty competition, the winning submission (Lainder & Wolfinger, 2022) employed gradient-boosted decision trees to generate probabilistic forecasts across a large retail hierarchy. In the related M5 Accuracy competition, the Direct Recursive Forecast Averaging via Partial Pooling model (DRFAM-PP; In & Jung, 2022) delivered strong point-forecast performance by combining direct and recursive strategies with pooled training datasets.

We extend DRFAM-PP from point to quantile forecasting, training direct and recursive learners as quantile models and averaging forecasts to obtain predictive distributions, thereby quantifying forecast uncertainty for downstream decision making. We replace fixed pooling with data-driven pooling set selection, casting pooling as a binary partitioning problem that endogenously opens pools from a candidate family using validation losses and a complexity-aware cost, allowing us to identify heterogeneous pools. We validate the approach in a real-world case at a German premium OEM, delivering probabilistic forecasts at the market–product-type level, a setting not yet addressed in the literature, and show that purely hierarchical pooling is empirically sub-optimal.

2.2. Spatiotemporal modeling

Traditional statistical time series regression models are adept at handling simple historical demand observations. However, they often struggle to capture the complexities inherent in multi-dimensional spatiotemporal correlated data (Liang et al., 2018). If OEMs can obtain prior infor-

mation regarding the demand distribution across various spatial areas and time intervals, they can better align supply with market demands.

The literature primarily focuses on spatiotemporal characteristics within transportation applications, employing ML approaches for modeling. Notable applications include transportation demand forecasting in car-hailing (Guo et al., 2022), bike-sharing (Yao et al., 2018; Gammelli et al., 2022), taxi traffic flow prediction (Ding et al., 2023), and ridesplitting (Li et al., 2024). For instance, Guo et al. (2022) proposed a forecasting approach that integrates spatial, temporal, and meteorological features. Experiments conducted on real-world data reveal that random forest regression, support vector regression, and k-nearest neighbor regression achieve the highest forecast accuracy. Li et al. (2024) employed multi-graph convolutional neural networks to extract spatiotemporal correlations among ride orders, demonstrating superior performance over single-graph architectures. Bi et al. (2022) proposed a retail sales forecasting approach at the store-product level, introducing a temporal latent factor model that achieves accurate predictions through a single tensor factorization across multiple stores and products.

While spatiotemporal modeling has been widely applied in urban transportation and retail contexts, existing research has primarily focused on local proximities (e.g., cities or stores within regions). In contrast, real-world industrial problems in the automotive sector involve multi-market and multi-product structures, where correlations arise not only from geography but also from shared economic conditions, product availability, and synchronized marketing strategies. Such cross-market interactions remain seldom addressed in the forecasting literature. This study extends spatiotemporal modeling to settings where markets are economically or behaviorally aligned rather than geographically adjacent, thereby moving beyond traditional locality-based assumptions.

2.3. Hierarchical forecasting

Base forecasts in hierarchical time series can be generated using local or global models. Local models capture series-specific patterns but become computationally intensive as the hierarchy expands, whereas global models exploit cross-series information and generally achieve higher accuracy and scalability (Montero-Manso & Hyndman, 2021).

Once base forecasts are generated, reconciliation methods are used to ensure coherence across the hierarchy. Comprehensive reviews of forecast reconciliation methods can be found in Athanasopoulos et al. (2024), Hollyman et al. (2021), and specifically for demand forecast reconciliation,

Babai et al. (2022). Traditional single-level reconciliation approaches such as bottom-up (BU), top-down (TD), and middle-out (MO) reconcile forecasts by either aggregating or disaggregating series. However, these methods rely on limited information from a specific hierarchical level and have shown limited robustness over time (Anderer & Li, 2022).

To address the limitations of single-level methods, least squares and optimization-based reconciliation techniques have gained popularity. Hyndman et al. (2011) forecast each level independently and then use ordinary least squares (OLS) to optimally combine the forecasts, which was later extended to a weighted least squares (WLS) solution (Hyndman et al., 2016) that weights series by the variance of the base forecast. Wickramasuriya et al. (2019) introduced an optimization strategy that minimizes the trace (MinT) of the covariance matrix of forecast errors, encompassing both OLS and WLS as special cases. While these methods assume unbiased base forecasts, Ben Taieb & Koo (2019) proposed an empirical risk minimization approach that minimizes the average squared error between reconciled forecasts and actual values, achieving competitive accuracy relative to benchmark methods under the unbiasedness assumption. However, traditional methods like OLS, WLS, and MinT do not guarantee non-negativity of reconciled forecasts, which can be addressed through constrained quadratic programming (e.g., Wickramasuriya et al., 2020).

Most reconciliation methods yield continuous forecasts, which are unsuitable for planning contexts that require integer decisions such as material requirements planning, car sequencing, and dealer order promising. This is critical for premium OEMs, where demand at the market-product type level involves low volumes and high variance. Rounding fractional reconciled forecasts both breaks hierarchical coherence and distorts planning, since even a ± 1 unit error can misrepresent a substantial share of demand and lead to costly buffers in parts inventory and production capacity. To address this, we propose a MILP formulation for discrete forecast reconciliation that is less complex, computationally efficient compared to existing approaches (e.g., Zhang et al., 2024), and yields forecasts that are both hierarchical consistent and operationally feasible. Our approach is decision-focused and follows empirical risk minimization in the hierarchical setting (Ben Taieb & Koo, 2019): it minimizes an out-of-sample average weighted L_1 loss with series-reliability and level-importance weights, thereby protecting stable aggregates while shifting adjustments to noisier components. Geometrically, it is the weighted- L_1 analogue of MinT on the integer coherent set; its LP relaxation recovers continuous L_1 reconciliation on the coherent cone, and under a quadratic

loss with base-error covariance it connects to MinT, reducing to OLS when the covariance is proportional to the identity matrix. Beyond integrality, the formulation can be extended to incorporate domain-specific linear constraints (e.g., forecast immutability), making it applicable across domains and allowing reconciliation and feasibility to be addressed within a single optimization.

2.4. Life cycle dynamics

The dynamic nature of product life cycles introduces significant complexity to the forecasting process (with automotive manufacturing as a documented example; Georgiadis et al., 2006).

While early model-based approaches used differential equations to describe product adoption (e.g., Kurawarwala & Matsuo, 1996; Lotfi et al., 2022), recent studies have shifted toward data-driven methods. Hu et al. (2018) fit product life cycle (PLC) curves to historical data, clustering similar patterns and identifying fourth-order polynomials as the best fit. Similarly, Elalem et al. (2023) employ data-driven time series clustering and explored ML approaches for PLC fitting. Their results suggest that while autoregressive integrated moving average models with exogenous inputs (ARIMAX) outperform deep neural networks in terms of mean absolute errors, the latter demonstrate robust performance under noisy data conditions. In contrast, Gonçalves et al. (2021) report that ARIMAX models provide higher accuracy during the early stages of the PLC, whereas ML models excel in later stages, indicating that deep learning is not uniformly superior. Guo et al. (2024) propose an ensemble that combines Bayesian model averaging with an exponential-smoothing life-cycle component, which adapts to recent changes and outperforms ML and Bayesian updating methods in forecasting the full demand distribution of new products.

Across industries, product life cycles occur as items are introduced, updated, and ultimately withdrawn (e.g., electronics, pharmaceuticals, software, media, manufacturing). Prior studies (e.g., Guo et al., 2024; Hu et al., 2018; Lotfi et al., 2022) often impose parametric PLC shapes (e.g., polynomial functions, Bass diffusion) and cluster pre-shaped trajectories, thereby limiting adaptability to the heterogeneous, multi-peak patterns driven by product updates and market shocks. Moreover, the studies reviewed operate at a single level, with PLC features defined per item, which restricts higher-level models from exploiting fine-grained temporal dynamics observed at lower levels. In contrast, we adopt a shape-agnostic, domain-neutral representation: the age-volume moment (AVM), defined as the product of time-since-introduction and realized volume. AVM requires only an introduction date and an observable measure of volume (e.g., units, downloads, prescriptions, streams)

and is additive across the hierarchy, enabling consistent learning across items, product lines, and markets without imposing a predefined PLC curve.

2.5. User-generated online information

In the automotive industry, user-generated online information, such as website traffic and online search trends, has gained increasing attention for demand forecasting, as manufacturers and dealers seek to better capture consumer preferences and behaviors. However, the existing literature provides mixed evidence on its effectiveness. For instance, Du et al. (2015) utilized online search trends to forecast car demand in the U.S. automotive market, demonstrating substantial improvements in model fit. Similarly, Fantazzini & Toktamysova (2015) developed multivariate models that integrate economic indicators and Google Search data to predict monthly car sales for several German OEMs. Their results indicate that models incorporating online information consistently outperform benchmark models that do not include such data across various car brands and forecast horizons. Zhang et al. (2022) used online reviews and search engine data to forecast aggregated product-level automobile sales, converting reviews into sentiment scores and training a backpropagation neural network, which significantly improved forecast accuracy and robustness.

In contrast, Schaer et al. (2019) critically assess studies such as Du et al. (2015) and Fantazzini & Toktamysova (2015), highlighting key design weaknesses (e.g., the absence of adequate benchmark models). They caution against overestimating the value of online information for operational decision-making. Notably, their findings show that in some cases, simple univariate time series models can outperform more complex models that incorporate online data, raising important questions about the robustness and practical value of these behavioral information sources.

No prior research has used online car configurator data to predict automotive demand, leaving a clear gap in the literature. We address this gap by introducing configurator interactions as a novel source of user-generated information for demand forecasting. Our contribution is twofold: first, we statistically evaluate the predictive value of configurator data and demonstrate its ability to enhance forecast accuracy when integrated into existing models; second, we apply XAI techniques to interpret how configurator usage patterns relate to future demand, providing transparent and actionable insights for decision-makers.

3. Automobile demand forecasting

3.1. Modeling

We formulate the task of predicting automobile demand as a multivariate, multi-step time series forecasting problem. Let $\{\mathbf{y}_t\}_{t=1}^T = \{\mathbf{y}_1, \mathbf{y}_2, \dots, \mathbf{y}_T\}$ represent the automobile demand time series (dependent variable) and $\{\mathbf{x}_t\}_{t=1}^T = \{\mathbf{x}_1, \mathbf{x}_2, \dots, \mathbf{x}_T\}$ denote the exogenous series (independent variable) over the past T time periods. Here, $\mathbf{y}_t = \{y_t^1, y_t^2, \dots, y_t^n\} \in \mathbb{R}^n$ defines a vector of demand values for n different time series in period t. Similarly, $\mathbf{x}_t = \{\mathbf{x}_t^1, \mathbf{x}_t^2, \dots, \mathbf{x}_t^n\} \in \mathbb{R}^{n \times m}$ defines a vector of m exogenous variables (features, covariates, independent variables) in period t. We approximate the unknown relationship between the dependent variable and its covariates by developing a forecasting model $f(\cdot)$, trained on the dataset $\mathcal{D} = \{(\mathbf{y}_t, \mathbf{x}_t)\}_{t=1}^T$. The objective is to minimize the difference between the observed values and the model predictions:

$$\{\hat{\mathbf{y}}_t\}_{t=T+1}^{T+H} = \{\hat{\mathbf{y}}_{T+1}, \hat{\mathbf{y}}_{T+2}, \dots, \hat{\mathbf{y}}_{T+H}\} = f(\{\mathbf{y}_t\}_{t=1}^T, \{\mathbf{x}_t\}_{t=1}^T; \theta),$$
(1)

where H is the forecast horizon and θ is a parameter vector of the model $f(\cdot)$.

While point forecasts provide a single expected value for future demand, they do not capture the uncertainty inherent in real-world forecasting tasks. To address this limitation, quantile forecasting enables the estimation of the distribution of automobile demand. We define the predicted automobile demand $\{\hat{\mathbf{y}}_t^q\}_{t=T+1}^{T+H} = \{\hat{\mathbf{y}}_{T+1}^q, \hat{\mathbf{y}}_{T+2}^q, \dots, \hat{\mathbf{y}}_{T+H}^q\}$ for a given quantile $q \in (0,1)$ as follows:

$$\left\{\hat{\mathbf{y}}_{t}^{q}\right\}_{t=T+1}^{T+H} = \left\{\inf\left(\mathbf{y}_{t} \in \mathbb{R}^{n} : q \leq \hat{F}(\mathbf{y}_{t}|\mathbf{y}_{1}, \dots, \mathbf{y}_{t-1}, \mathbf{x}_{t})\right)\right\}_{t=T+1}^{T+H},$$
(2)

where $\hat{F}(\cdot)$ denotes the estimated cumulative distribution function of the conditional distribution $\mathbb{P}(\mathbf{y}_t|\mathbf{y}_1,\ldots,\mathbf{y}_{t-1},\mathbf{x}_t)$ in period t. The distribution $\mathbb{P}(\cdot)$ is conditioned on the autoregressive parts $\mathbf{y}_1,\ldots,\mathbf{y}_{t-1}$ and exogenous variables \mathbf{x}_t . Thus, we can investigate the influence of explanatory variables on the shape of the demand distribution. To provide a comprehensive view of the distribution, we focus on the median and prediction intervals (PIs) at the 50%, 67%, 95%, and 99% levels by investigating a set of quantiles $\mathcal{Q} = \{0.005, 0.025, 0.165, 0.25, 0.5, 0.75, 0.835, 0.975, 0.995\}$. The median, along with the 50% and 67% PIs, capture the central tendency and short-term uncertainty of automobile demand. This information is useful for monthly vehicle allocation decisions, where manufacturers must balance limited supply against expected regional demand to minimize inventory costs and lost sales. The 95% and 99% PIs provide insight into the extreme tails of the

distribution. Their upper and lower bounds are crucial for risk assessment and capacity planning, enabling stakeholders to prepare for rare but impactful demand fluctuations.

3.2. Pooling strategies

Pooling combines information across related time series to improve forecast accuracy. In practice, this spans local models (no pooling), global models (full pooling), and intermediate partial pooling along structured groups. Recent work (Montero-Manso & Hyndman, 2021) reframes pooled forecasting as a partitioning problem on the local—global spectrum, where the granularity of the partition governs model complexity and generalization and should be learned from data rather than fixed a priori.

We therefore formulate pooling as a data-driven partitioning problem: series are assigned to pools that share one forecast model, trading off empirical accuracy and model complexity. Let \mathcal{I} be the set of series and \mathcal{G} a finite family of candidate pools, with $g \subseteq \mathcal{I}$. The candidate family integrates hierarchy-derived groups (e.g., market-product cluster), domain categories (e.g., fuel and body type), data-driven clusters, and their combinations. To guarantee coverage and a no-pooling fallback, we include all singletons $\{i\}$ (local models), so that every $i \in \mathcal{I}$ belongs to at least one $g \in \mathcal{G}$. For each admissible pair (i,g) with $i \in g$, we compute a leakage-safe rolling-origin cross-validated loss L_{ig} on validation folds only. Each pool g incurs an opening cost κ_g that penalizes (i) the number of models induced by the grouping (computational complexity) and (ii) within-group sample imbalance (overfitting risk).

We define the pooling selection as a binary partitioning problem (POOL-SEL-BP):

$$\min_{x \in \{0,1\}^{\mathcal{I} \times \mathcal{G}}, y \in \{0,1\}^{\mathcal{G}}} \sum_{i \in \mathcal{I}} \sum_{q \in \mathcal{G}: i \in q} L_{ig} x_{ig} + \lambda \sum_{q \in \mathcal{G}} \kappa_g y_g, \tag{3}$$

s.t.

$$\sum_{g \in \mathcal{G}: i \in g} x_{ig} = 1, \quad \forall i \in \mathcal{I}, \tag{4}$$

$$x_{ig} \le y_g, \quad \forall i \in \mathcal{I}, g \in \mathcal{G},$$
 (5)

with $\lambda \geq 0$ trading off accuracy and complexity. The selected pooling families and the exact pool-cost specifications are provided in the e-companion (EC.3).

3.3. Forecasting strategies and ensemble construction

We consider three multi-step forecasting strategies, denoted as $S = \{DIR, REC, HYB\}$. Each generates forecasts at horizon $h \in [1, H]$, using only information available up to T. All strategies are trained separately for each quantile $q \in Q$, enabling distributional forecasts without altering the underlying model structure.

Direct forecasting (DIR) trains a separate model for each forecast horizon:

$$\hat{\mathbf{y}}_{T+h}^{\text{DIR}} = f_h(\mathbf{y}_{1:T}, \mathbf{x}_T; \theta_h), \tag{6}$$

where $f_h(\cdot)$ is a horizon-specific model with parameters θ_h . This strategy avoids error accumulation but does not enforce temporal consistency across horizons (Ben Taieb et al., 2012). Recursive forecasting (REC) trains a single one-step-ahead model and recursively uses previous forecasts as inputs:

$$\hat{\mathbf{y}}_{T+h}^{\text{REC}} = f(\overline{\mathbf{y}}_{T+h-1}, \overline{\mathbf{x}}_{T+h-1}; \theta), \tag{7}$$

where $\overline{\mathbf{y}}_{T+h-1} = \{\mathbf{y_1}, \dots, \mathbf{y_T}, \mathbf{\hat{y}}_{T+1}^{\text{REC}}, \dots, \mathbf{\hat{y}}_{T+h-1}^{\text{REC}}\}$ denotes the sequence of observed and predicted targets, and $\overline{\mathbf{x}}_{T+h-1}$ are the corresponding exogenous features, replacing unknown values with forecasts when needed. While compact and efficient, REC suffers from error accumulation (Ben Taieb et al., 2012). Hybrid forecasting (HYB) combines the strengths of DIR and REC by training a separate model for each horizon while incorporating lagged forecasts as autoregressive inputs:

$$\hat{\mathbf{y}}_{T+h}^{\text{HYB}} = f_h(\overline{\mathbf{y}}_{T+h-1}, \mathbf{x}_T; \theta_h). \tag{8}$$

HYB (often referred to as DirRec) combines the horizon-specific modeling flexibility of DIR with the temporal dependency modeling of REC. As shown in Ben Taieb et al. (2012), such hybrid models can reduce cumulative forecast errors while preserving temporal structures. To further improve prediction accuracy and robustness, we define an ensemble model (ENS) that averages forecasts from all strategies in S:

$$\hat{\mathbf{y}}_{T+h}^{\text{ENS}} = \frac{1}{|\mathcal{S}|} \sum_{s \in \mathcal{S}} \hat{\mathbf{y}}_{T+h}^{s}$$
(9)

By combining forecasts from diverse models, ENS leverages their complementary strengths to reduce variance and mitigate individual model biases (Breiman, 1996).

Model diversity is key to ensemble effectiveness (Brown et al., 2005). To further enhance this, we include a pooled ensemble based on hierarchical pooling (DRFAM-PP (HIER)) and optimal

pooling selection via POOL-SEL-BP (DRFAM-PP (OPT)). We define the DRFAM-PP forecast for series i at horizon h as the average of direct and recursive forecasts across all active pools that include series i:

$$\hat{\mathbf{y}}_{i,T+h}^{\text{DRFAM-PP}} = \frac{1}{|\mathcal{S}_{\text{DR}}||\mathcal{G}_i|} \sum_{s \in \mathcal{S}_{\text{DR}}} \sum_{g \in \mathcal{G}_i} \hat{\mathbf{y}}_{T+h}^{s,g}, \tag{10}$$

where $S_{DR} = \{DIR, REC\}$ denotes the set of included forecasting strategies, $G_i = \{g \in G | i \in g, y_g = 1\}$ is the set of active pools containing series i, and $\hat{\mathbf{y}}_{T+h}^{s,g}$ is the forecast at horizon h from strategy s trained on the pooled dataset \mathcal{D}_g . HYB models are excluded from DRFAM-PP to remain consistent with its original definition. However, we evaluate them separately and also include them in broader ensemble benchmarks.

3.4. Forecast reconciliation

Forecast reconciliation ensures that disaggregated automobile demand forecasts (e.g., market-product type) are coherent with their aggregates (brand, market). Following Hyndman et al. (2011), reconciled forecasts can be written as $\tilde{\mathbf{y}}_t = \mathbf{SG}\hat{\mathbf{y}}_t$. Here, $\tilde{\mathbf{y}}_t$ denotes the reconciled vector at horizon t; $\mathbf{S} \in \{0,1\}^{N \times B}$ is the structural/summing matrix that maps the B bottom-level series to all N series (so the coherent subspace is $s = \operatorname{col}(\mathbf{S})$); and matrix $\mathbf{G} \in \mathbb{R}^{B \times N}$ defines the reconciliation weights and determines how base forecasts $\hat{\mathbf{y}}$ are adjusted to ensure coherence across the hierarchy. Classical methods (e.g., MinT) can then be interpreted as weighted L_2 projections of the base forecasts onto the coherent subspace s, and, when non-negativity is imposed, onto the coherent cone $K = s \cap \mathbb{R}^N_{\geq 0}$ (Panagiotelis et al., 2021). We adopt the same geometric lens, but change both the metric and the support: we use a weighted L_1 distance and restrict the solution to the integer lattice inside the cone $K_{\mathbb{Z}} = K \cap \mathbb{Z}^N = (s \cap \mathbb{R}_{\geq 0}) \cap \mathbb{Z}^N$. The geometric motivation and a side-by-side comparison with OLS and MinT are further illustrated in the e-companion EC.4.

In the automotive industry, forecasts must be non-negative and integer-valued, reflecting the discrete nature of vehicle production, inventory, and order fulfillment processes. In particular, integer forecasts are essential to avoid rounding errors in low-volume series and to ensure operational feasibility across product portfolios with highly variable demand scales. We therefore propose a mixed-integer linear programming reconciliation (REC-MILP) that finds the reconciled point closest to the base forecast in a level/series-weighted L_1 distance, while restricting the solution to the integer-coherent feasible set:

$$\min_{b_{jt} \in \mathbb{Z}_{\geq 0}, z_{it} \in \mathbb{R}_{\geq 0}} \frac{1}{NH} \sum_{i \in \mathcal{I}} \sum_{t \in \mathcal{T}} w_i z_{it}, \tag{11}$$

s.t.

$$z_{it} \ge \sum_{i \in \mathcal{B}} s_{ij} b_{jt} - \hat{y}_{it} \quad , \forall i \in \mathcal{I}; t \in \mathcal{T},$$
 (12)

$$z_{it} \ge \hat{y}_{it} - \sum_{j \in \mathcal{B}} s_{ij} b_{jt} \quad , \forall i \in \mathcal{I}; t \in \mathcal{T}.$$
 (13)

Let \mathcal{I} denote the set of all series across all hierarchy levels ($|\mathcal{I}| = N$), \mathcal{B} the set of bottom-level series $(|\mathcal{B}| = B)$, and $\mathcal{T} = \{T+1, \dots, T+H\}$ the forecast horizons. Decision variables are bottomlevel reconciled forecasts $b_{jt} \in \mathbb{Z}_{\geq 0}$. Absolute deviations from the base forecasts are captured by auxiliary variables $z_{it} \in \mathbb{R}_{\geq 0}$. Objective (11) minimizes the sample-average of weighted absolute errors, so REC-MILP can be read as empirical risk minimization over the class of integer-coherent forecasts. Constraints (12)–(13) linearize the absolute error term and reconciled values at any level follow from bottom-level decisions via $\tilde{y}_t = (\mathbf{S}b_t)_i$. The weights w_i control how strongly deviations from the base forecast are penalized. In our baseline REC-MILP, we set $w_i = \gamma_i$ to reflect seriesspecific reliability (e.g., $\gamma_i = 1/WMAPE_i$ or other accuracy-based proxy). A higher γ_i penalizes deviations from reliable base forecasts more strongly, preserving their accuracy. Conversely, a lower γ_i allows greater adjustments in less trustworthy forecasts, promoting corrections where base models underperform. In the level-weighted variant (REC-LW-MILP), we set $w_i = \gamma_i \alpha_{l(i)}$, where l(i) maps each series to its level $l \in \mathcal{L}$, and $\alpha_l \geq 0, \sum_{l \in \mathcal{L}} \alpha_l = 1$, encode managerial priorities across the hierarchy. For instance, demand at higher aggregation levels (e.g., brand or market) carries greater managerial importance, whereas lower levels (e.g., product type) are critical for operational feasibility though typically noisier. This level-weighted design provides flexibility by allowing decision-makers to emphasize different hierarchy levels depending on the planning task.

4. Case study

4.1. Data

The dataset was provided by a German premium OEM and comprises approximately 190,000 monthly observations of actual orders for a single brand. The observation period covers 12 years in total. The training set spans Years 1–11, the validation set (used for hyperparameter optimization)

covers Years 9–11, and the test set corresponds to Year 12. The dataset is detailed at the market-product type level, encompassing 4,386 time series across 23 markets and 501 product types. These time series can be aggregated across a four-level product hierarchy, which is defined by Brand, Product Cluster, Product Line, and Product Type (Table 1).

ID	Level	Description	# Time series
0	Brand	Total brand orders	1
1	Market	Total orders, aggregated for each market	23
2	Market–Product Cluster	Total orders, aggregated for each market and product cluster	115
3	Market–Product Line	Total orders, aggregated for each market and product line	412
4	Market–Product Type	Total orders, aggregated for each market and product type	4,386

Table 1: Number of time series per hierarchy level and corresponding level descriptions.

Notes. High levels of aggregation correspond to low identification numbers (IDs) (e.g., levels 0 and 1), while low levels of aggregation correspond to higher IDs (e.g., levels 2 and 3), with level 4 being the most granular level.

Within the dataset, each product type is characterized by several attributes (e.g., body type, fuel type, transmission, performance, number of doors and cylinders, and life cycle age). These attributes will henceforth be referred to as master data. In addition to the master data, the set of explanatory variables is extensive, incorporating publicly available macroeconomic data extracted from Eurostat and stock market data retrieved from Yahoo Finance (see Table EC.4 of e-companion EC.6.1), as well as company-internal information such as configurator website visits, inventory levels, sales targets, and pricing-related variables.

The forecasting horizon was set to six months to align with the company's short- to mediumterm planning cycles. This supports operational and tactical decisions such as adjusting production, managing inventory, and monitoring alignment with sales targets, while providing sufficient lead time for supplier and logistics coordination. We employed a six-month rolling horizon forecasting approach, retraining the models at each period, resulting in seven test windows.

4.2. Exploratory data analysis

Spatiotemporal data characteristics across hierarchical levels. Table 2 shows that the share of stationary series increases with granularity, reaching nearly 46% at the Market-Product Type level. Stationarity was assessed using the Augmented Dickey-Fuller test, applied individually to each time series. The Brand level aggregate displays strong non-stationarity, capturing long-term trends and seasonality. In contrast, at the lowest aggregation level, nearly half of the time

series show stationarity. This shift in stationarity suggests that forecasting models must adapt their assumptions regarding trends, differencing requirements, and error structures by hierarchical level (RQ1). At aggregated levels, models should emphasize trend and seasonal components, while at lower levels, capturing local variability is more important.

Autocorrelation was tested using the Breusch-Godfrey test for both first- and third-order serial correlation. The analysis reveals strong temporal dependencies: the single Brand-level series in our sample exhibited autocorrelation up to lag 3, while at the Market level nearly 87% of series did so. At the Market-Product Type level, about 58% showed autocorrelation at this order. Partial autocorrelations at lags 1, 2, and lag 13 suggest both short-term persistence and annual seasonal effects (see Figure EC.4 of e-companion EC.6.3). Forecasting approaches need to incorporate these short-term and seasonal dependencies explicitly to improve accuracy (RQ1, RQ2).

Spatial correlations, examined via the cross-correlation function, reveal that demand fluctuations in different markets are synchronized at lag 0, indicating simultaneous influence by shared external drivers such as economic shifts or marketing campaigns (see Figure EC.4 of e-companion EC.6.3). This spatial interaction must be modeled to capture cross-market dependencies and improve hierarchical forecasting (RQ1, RQ2).

Level	Stationarity	Autocorrelation		Demand	classification		
		First-order	\leq Third-order	Smooth	Intermittent	Erratic	Lumpy
0: Brand	0.00	100.00	100.00	100.00	0.00	0.00	0.00
1: Market	39.13	86.96	100.00	73.91	0.00	26.09	0.00
2: Market–Product Cluster	37.39	73.04	79.13	42.60	0.00	57.40	0.00
3: Market–Product Line	36.89	56.79	62.86	28.15	0.00	71.85	0.00
4: Market–Product Type	45.96	56.49	58.23	20.70	0.00	79.30	0.00

Table 2: Percentage of time series per level by stationarity, autocorrelation, and demand classification.

Demand classification and variability. Applying the Syntetos et al. (2005) framework shows that demand becomes smoother at higher aggregation levels, while erratic behavior increases considerably at more granular levels (Table 2). At the lowest level, nearly 80% of series exhibit erratic demand patterns. Intermittent and lumpy demand patterns are not present in the data. Erratic demand at granular levels reflects diverse customer choices and localized market effects, increasing forecasting complexity and uncertainty. This aligns with existing literature reporting erratic demand patterns in manufacturing products (Geng et al., 2009; Onyeocha et al., 2015). Hence,

models must accommodate this variability, possibly through robust error structures or probabilistic approaches, to maintain forecast reliability (RQ1, RQ2).

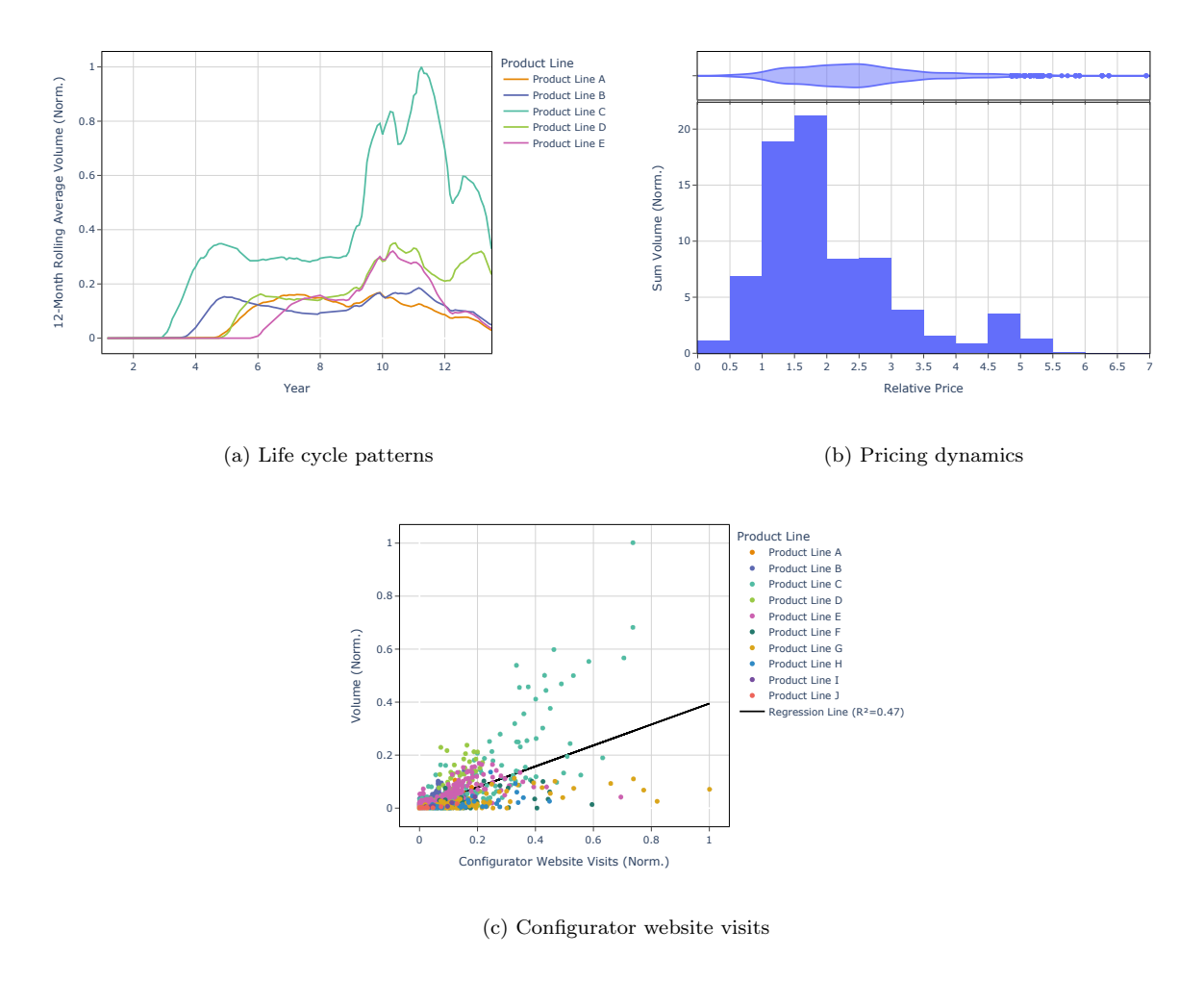


Figure 1: Summary plots for exploratory data analysis (Market-Product Line level).

Product life cycles. Figure 1a presents life cycle volumes at the Market-Product Line level. Life cycles typically last 5–7 years, though with notable deviations from classical PLC models. Instead of a smooth introduction-growth-maturity-decline trajectory, the data reveal multiple demand peaks during maturity phases, linked to product innovations and technical updates. The complex, multi-peak life cycle patterns indicate that demand is strongly driven by product innovation timing and market acceptance dynamics rather than simple linear progression. Thus, accurate forecasting requires models that integrate product life cycle stages as core predictors (RQ2).

User-generated online information. In the automotive industry, which is dominated by wholesale-centered, indirect sales models, OEMs have limited visibility into actual customer purchasing behavior. User-generated data, such as configurator website visits, therefore provides valuable customer- and product-specific signals that would otherwise be unavailable. Regression analysis shows that configurator visits explain about 47% of demand variance at the Market-Product Line level (Figure 1c) but only 30% at the Market-Product Type level. Hence, car configurator visits provide valuable signals that can enhance demand forecasts (RQ3), improving early detection of demand shifts and supporting responsive marketing decisions.

Price influence on demand. Analysis of relative pricing (Market–Product Line average price divided by Market–Product Cluster average price) against cumulative volume (Figure 1b) reveals distinct demand peaks between price ratios of 1.5–2.0, indicating a perceived optimal value range. Demand declines below 1.5 and above 2.0, reflecting customer behavior with possible quality concerns or due to price sensitivity. A secondary demand peak appears between 4.5–5.0, suggesting premium segment behavior, where customers are willing to pay a premium for perceived quality, exclusivity, or brand prestige, reflecting behaviors associated with Veblen goods. Thus, price sensitivity and segment-specific demand elasticity are influential explanatory variables for automobile demand forecasting (RQ2).

4.3. Benchmark models

We benchmark DRFAM-PP against both statistical and ML-based methods. All models are trained separately for each quantile. Due to data sparsity at higher aggregation levels, the following methods are applied only at the Market-Product Type level: DRFAM-PP (with pooled LightGBM base models), DeepAR (Salinas et al., 2020), and NBEATSx (Olivares et al., 2023). Importantly, we run two DRFAM-PP variants: i) hierarchical pooling, using the exogenously defined hierarchy with pools at the Market, Market-Product Cluster, and Product Line levels (DRFAM-PP (HIER)); and (ii) optimal pooling via POOL-SEL-BP, which endogenously selects pools (DRFAM-PP (OPT)). For the latter, the selected pools are body type, market, and market cluster (see e-companion EC.3 for selection details). All other forecasting strategies are implemented across the full hierarchy. Specifically, DIR, REC, HYB, and their ensemble ENS are implemented using global LightGBM models. In addition, we include six statistical baselines: naive, seasonal naive (sNaive), moving average (MA), exponential smoothing (ETS), ARIMA, and Prophet (Taylor & Letham, 2018).

4.4. Feature engineering, data processing, and model tuning

Feature engineering extends baseline covariates with two domain-neutral interaction terms: (i) the age-volume moment (AVM), linking demand to product maturity, and (ii) a web-traffic-demand interaction (WDI), capturing the joint intensity of digital attention and demand. To prevent leakage, both use a one-sided k-period smoother $S_k(\cdot)$ computed with information up to t-1; in our implementation, we set k=3 and use a trailing moving average. For series i at time t with introduction date s_i , let age $a_{it}=t-s_i$. The AVM is $AVM_{it}=a_{it}S_k(y_{i,\leq t-1})$. AVM is additive across the hierarchy, aggregating by simple summation to level l: $AVM_{lt}=\sum_{i\in\mathcal{I}:l(i)=l}AVM_{it}$. Let v_{it} denote online visits for series i at time t. The WDI is $WDI_{it}=S_k(v_{i,\leq t-1})S_k(y_{i,\leq t-1})$ and aggregates analogously: $WDI_{lt}=\sum_{i\in\mathcal{I}:l(i)=l}WDI_{it}$.

We preselect features using the Maximum Relevance Minimum Redundancy algorithm (Ding & Peng, 2003), trained on mutual information, to identify m=40 explanatory variables for each forecast horizon. Selecting 40 variables strikes a balance between capturing sufficient explanatory power and avoiding overfitting or instability in interpretation. The union of all selected features is reported in the e-companion (EC.6.2, Table EC.5). This preselection is crucial for minimizing the risk of potentially misleading Shapley Additive Explanations (SHAP) values, as high correlations among features can lead to imprecise interpretations and even opposite signs (Aas et al., 2021), contrary to the original assumption of feature independence made by Lundberg & Lee (2017).

To address extrapolation limitations of tree-based models, we apply first-order differencing to all time series, and quantile-transform the target variable to approximate normality. Temporal features are encoded with one-hot variables for year and quarter, and sinusoidal transformations for month and month-of-quarter. Categorical predictors are one-hot encoded when categories are few; otherwise, high-cardinality features are handled using LightGBM's native categorical encoding (Ke et al., 2017) or frequency encoding for deep learning models. Numerical features are standardized, and two principal components are extracted to reduce dimensionality. Missing values are encoded with -1 for tree-based models, while deep learning models use forward- and backfilling strategies.

Hyperparameters are optimized with *Optuna* 4.1 using four-fold cross-validation on a 2-year validation set, with each fold covering six months. The tuning process is guided by root mean squared error. Implementation details, including hardware specifications and library versions, are reported in the e-companion (EC.1); hyperparameter settings in EC.6.4 (Table EC.6).

4.5. Forecast error assessment

To assess forecast accuracy, we adopt a two-step process similar to that used in the M5 Accuracy competition: errors are first averaged over the forecast horizon for each time series, then across all series. This process is applied at each hierarchical level. We omit revenue-based weighting, as it can distort results; volume-based precision is crucial for the OEM in tasks such as production planning.

4.5.1. Point forecast

Root mean squared scaled error (RMSSE) is used to compare forecast accuracy across models within each hierarchical level:

$$RMSSE = \sqrt{\frac{\frac{1}{H} \sum_{t=T+1}^{T+H} (y_t - \hat{y}_t)^2}{\frac{1}{T-1} \sum_{t=2}^{T} (y_t - y_{t-1})^2}}.$$
 (14)

RMSSE is scale-independent, allowing fair comparison between series with different magnitudes or volatility; it is symmetric; and it can be computed safely, as it does not depend on values that may be equal to or close to zero (Makridakis et al., 2022a). To complement RMSSE, weighted mean absolute percentage error (WMAPE) is used for cross-level comparison:

$$WMAPE = \frac{\sum_{t=T+1}^{T+H} |y_t - \hat{y}_t|}{\sum_{t=T+1}^{T+H} |y_t|}.$$
 (15)

WMAPE is intuitive, expressing error as a percentage of actual values and useful for comparing aggregate accuracy across hierarchical levels.

To detect systematic directional errors, we additionally report the (scaled) Forecast Bias (FB):

$$FB = \frac{\sum_{t=T+1}^{T+H} (y_t - \hat{y}_t)}{\sum_{t=T+1}^{T+H} y_t}.$$
 (16)

FB helps detect consistent over- or under-forecasting: a positive bias indicates underestimation, which can lead to underproduction or understocking, and vice versa. While FB is useful for identifying directional bias, it does not reflect the magnitude of errors and is therefore used as a sanity check rather than a primary performance metric.

4.5.2. Probabilistic forecast

We employ the scaled pinball loss (SPL), which is computed for each time series and quantile as follows:

$$SPL(q) = \frac{\frac{1}{H} \sum_{t=T+1}^{T+H} [(y_t - \hat{y}_t^q) q \mathbb{1} \{ \hat{y}_t^q \le y_t \} + (\hat{y}_t^q - y_t) (1 - q) \mathbb{1} \{ \hat{y}_t^q > y_t \}]}{\frac{1}{T-1} \sum_{t=2}^{T} |y_t - y_{t-1}|},$$
(17)

where $\mathbb{1}\{\cdot\}$ is the indicator function that equals 1 if y_t falls within the specified interval, and 0 otherwise. Similar to the point forecast, the denominator is calculated only for periods with non-zero demand. The pinball loss function penalizes overestimation more heavily for low-probability quantiles, and underestimation more for high-probability quantiles. SPL is normalized similarly to the RMSSE, enabling consistent comparisons across time series with different scales. It is numerically stable, as it avoids divisions by values approaching zero. Moreover, to fairly estimate the distribution of forecast uncertainty, no weights are applied to the evaluated quantiles, ensuring an unbiased representation of uncertainty across the forecast distribution (Makridakis et al., 2022a). The mean SPL (MSPL) is obtained by averaging over all quantiles:

$$MSPL = \frac{1}{|\mathcal{Q}|} \sum_{q \in \mathcal{Q}} SPL(q).$$
 (18)

5. Results

5.1. Forecast method effectiveness

Table 3 compares point (RMSSE) and probabilistic (MSPL) forecast accuracy across hierarchical levels from Brand to Market–Product Type, including only the best-performing statistical benchmark (full statistical benchmark results are in Appendix A; extended accuracy metrics, including WMAPE and FB, are reported in the e-companion EC.5.6). The Market–Product Type level accuracy evaluation is further supported by Figure 2.

Level	Metric	Statistical	DeepAR	NBEATSx	DIR	REC	НҮВ	ENS	DRFAM-PP (HIER)	DRFAM-PP (OPT)
0: Brand	RMSSE	0.640	†	†	1.145	0.750	1.267	1.020	†	†
	MSPL	0.334	†	†	0.320	$\underline{0.233}$	0.292	0.240	†	†
1: Market	${\rm RMSSE}$	0.648	†	†	0.606	0.638	0.730	0.579	†	†
	MSPL	0.362	†	†	0.249	$\underline{0.202}$	0.217	0.206	†	†
2: Market–Product Cluster	${\rm RMSSE}$	0.608	†	†	0.621	0.618	0.804	0.546	†	†
	MSPL	0.390	†	†	0.229	0.206	0.257	0.200	†	†
3: Market–Product Line	${\rm RMSSE}$	0.579	†	†	0.521	0.543	0.675	$\underline{0.436}$	†	†
	MSPL	0.362	†	†	0.185	0.155	0.206	0.145	†	†
4: Market–Product Type	${\rm RMSSE}$	0.539	0.494	0.531	0.581	0.576	0.478	0.516	0.469	0.418
	MSPL	0.310	0.182	0.654	0.227	0.171	0.154	0.181	0.134	0.128

Table 3: Point and probabilistic forecast accuracy across hierarchical levels.

Notes. †: Insufficient data available for the application of the specified model. Underlined values indicate the best accuracy, while bold numbers represent values that are at most 5% worse than the best.

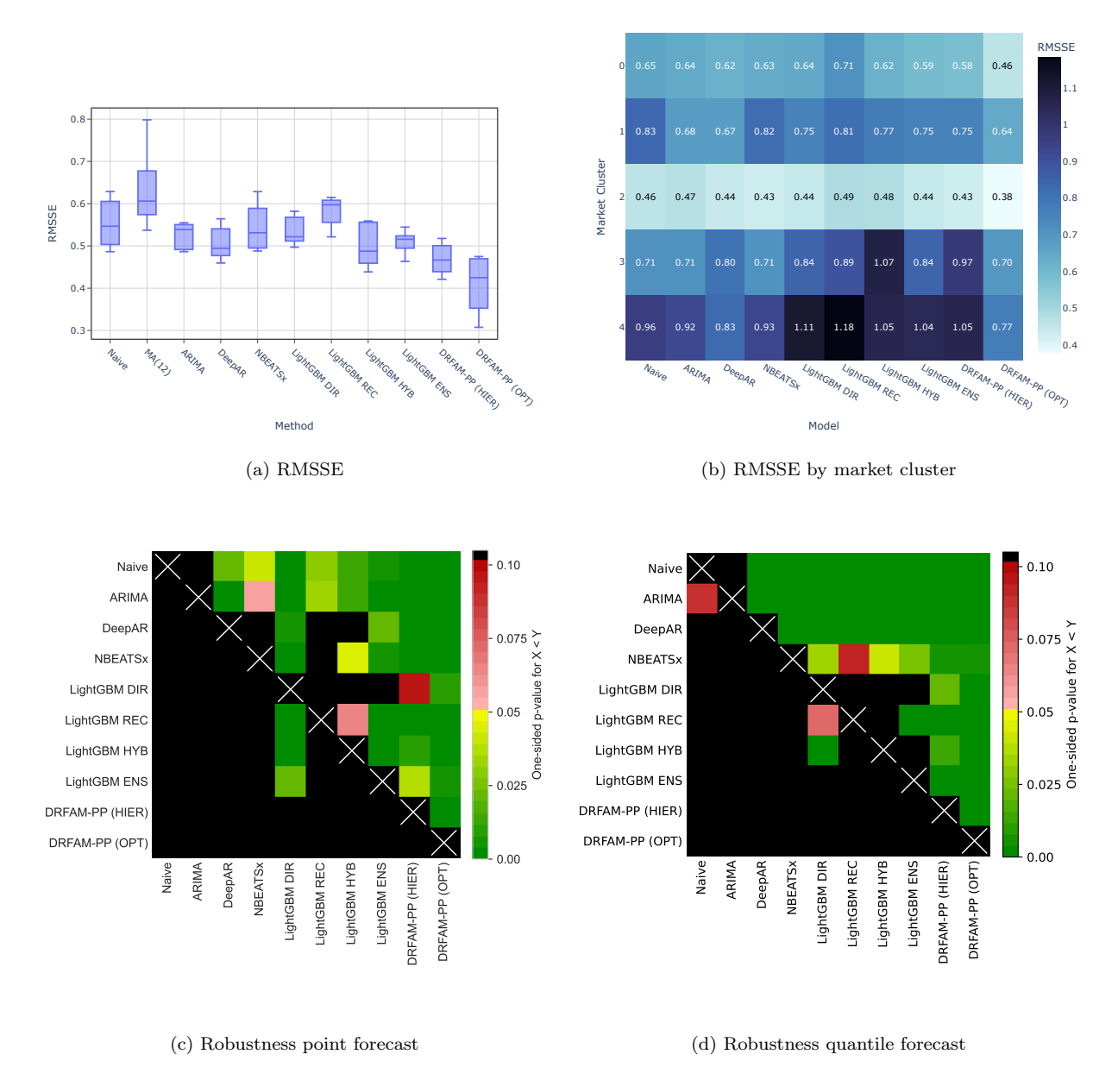


Figure 2: Summary plots for Market-Product Type level accuracy.

Notes. Panels (a), (b): report median scores calculated over the seven test periods. Panels (c), (d): Giacomini–White test; HAC (Newey–West) with lag L = H - 1; losses are MSE (c) and CRPS via trapezoidal approximation (d).

The main results related to RQ1 are summarized below (minor results are in e-companion EC.5). Brand level: simple statistical benchmarks yield the lowest RMSSE (0.640), consistent with stable aggregate patterns. LightGBM REC and ENS variants deliver the best probabilistic scores, reflecting their superior ability to quantify forecast uncertainty. Intermediate levels (1–3): ENS attains

the best point and probabilistic accuracy (improvements: RMSSE-15.24%, SPL-50.59% vs. best statistical baseline). Market-Product-Type level: DRFAM-PP (OPT) outperforms all benchmark methods in both point (Figure 2a) and probabilistic (see e-companion EC.6.6) accuracy, followed closely by LightGBM HYB and ENS variants. Robustness checks using Giacomini-White tests confirm these rankings (Figures 2c,d). Moreover, hierarchical pooling is empirically non-optimal: the tests favor optimal, data-driven pooling over fixed hierarchical pooling (DRFAM-PP (HIER)) in pairwise comparisons. Deep learning models (DeepAR, NBEATSx) perform competitively at level 4 but exhibit long-horizon overprediction bias (see e-companion EC.6.5), whereas both DRFAM-PP variants maintain stable bias across all forecast horizons and test periods.

Finding 1: Spatial heterogeneity of forecast performance. Accuracy gains from DRFAM-PP (OPT) are not spatially uniform but depend on market maturity, volume, and volatility (Figure 2b). The largest improvements occur in high-volume markets (clusters 0 and 1), where the economic stakes are highest, while in saturated markets (cluster 3) improvements over naive benchmarks were marginal. In growth-phase markets, forecast errors were higher across all models due to limited history and evolving dynamics; here DRFAM-PP (OPT) improved RMSSE by 3.65%, compared to more pronounced gains of 10.29% in mature markets. At the individual market level, DRFAM-PP (OPT) delivered top accuracy in 65% of cases, primarily in stable, high-sales environments. By contrast, global ensemble methods retained an edge in low-volume or rapidly evolving markets.

These patterns generalize beyond automotive to any multi-region, multi-segment demand system: forecasting performance varies with spatial structure and market phase, not just hierarchical level. A context-dependent deployment is therefore preferable to a uniform rollout: allocate resource-intensive models like DRFAM-PP (OPT) to mature, high-impact regions, and use faster-to-implement, adaptive global models where data are sparse or dynamics shift quickly. This suggests a hybrid strategy where model choice becomes context-dependent, aligning forecasting investment with economic return.

Finding 2: Rounding substantially impacts forecast accuracy, and MILP-based reconciliation outperforms benchmark methods. We compared REC-MILP and its level-weighted extension (REC-MILP-LW) against benchmark reconciliation methods (BU, MinT) and unreconciled base forecasts from ETS, ARIMA, and LightGBM REC. For BU and MinT, reconciliation was applied to continuous forecasts with post hoc rounding. Detailed methodological

explanations and complete result tables are provided in Appendix B.

Results show that rounding can meaningfully distort accuracy: at the Market–Product Type level (Figure 3a), rounding improved BU relative to unrounded base forecasts but generally increased error for BU and MinT at other levels (Appendix B, Tables B.8–B.7). By contrast, REC-MILP consistently avoided this degradation and in many cases matched or improved base forecast accuracy. The level-weighted variant (REC-MILP-LW) further demonstrated that targeting the objective to the Market–Product Type level improved bottom-level accuracy with only modest trade-offs at higher levels (Figure 3b; Appendix B, Table B.6). Gains were strongest for ARIMA and LightGBM REC, where variable forecasts across the horizon are more sensitive to rounding bias. In contrast, ETS produces constant forecasts over the horizon, limiting rounding effects; differences were small and statistically insignificant.

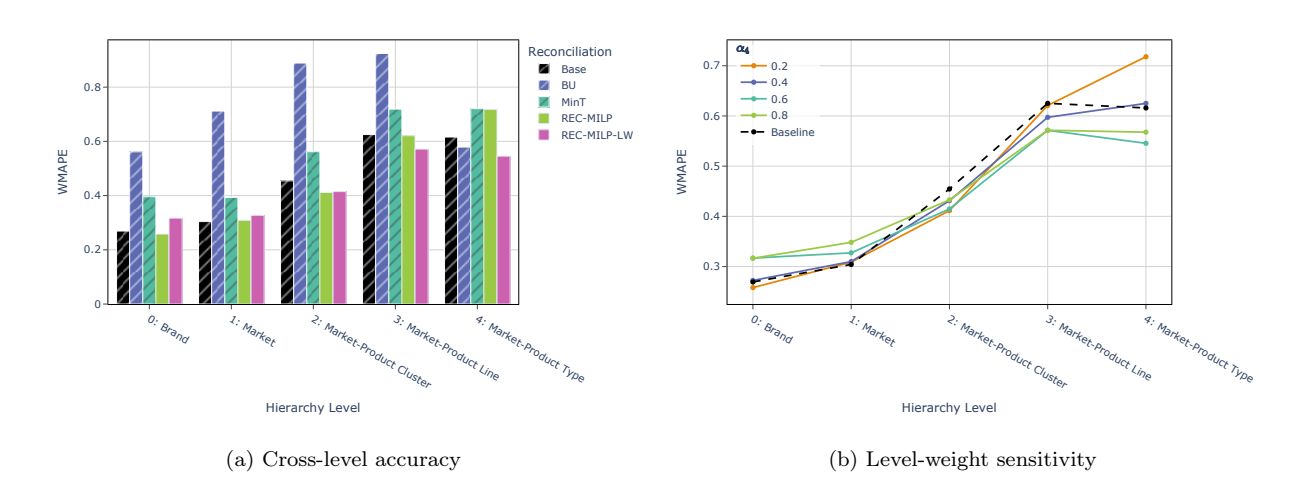


Figure 3: Forecast accuracy of reconciliation methods across hierarchical levels.

Notes. Figures show median WMAPE scores for the ARIMA base forecast. In panel (a), shaded bars indicate reconciliation methods that are non-coherent after integer-rounding.

From an applied forecasting perspective, these results underscore two implications. First, reconciliation is not only about achieving hierarchical coherence but also about operational implementability: integer bottom-level forecasts matter wherever plans translate directly into discrete production, inventory, or fulfillment decisions. Second, REC-MILP-LW offers practitioners a practical tuning mechanism: managers can assign weights to emphasize operational feasibility (e.g., production scheduling) or strategic alignment (e.g., brand/region planning). Importantly, the method

delivers robustness as it avoids accuracy losses where rounding has little impact, while producing the largest gains in settings where variance and rounding sensitivity are high. This makes integer-coherent reconciliation particularly valuable for industries characterized by low volumes, high product variety, or discrete production and allocation decisions (e.g., automotive, electronics, pharmaceuticals, and retail), where precise bottom-level forecasts help avoid costly overproduction, lost sales, or inefficiencies in sequencing and replenishment processes. In addition to its accuracy benefits, REC-MILP(-LW) also demonstrates competitive computational efficiency. In our study, MinT required approximately one hour to compute the reconciliation using a full shrinkage-based covariance estimate, while REC-MILP solved the integer optimization in seconds. This efficiency extends to solving reconciliation across full hierarchies and horizons simultaneously, making the method scalable to large industrial forecasting systems.

5.2. Predictors of automobile demand

We conducted a global SHAP analysis to identify the most influential predictors of automobile demand (RQ2) at the Market–Product Type level. SHAP values were computed using the Tree-SHAP algorithm. Figure 4 presents the distribution of SHAP values per feature for the 1-month and 6-month forecast horizons based on a direct LightGBM model. Although this model did not yield the highest accuracy in earlier comparisons, it offers strong interpretability, allowing us to examine how individual input features contribute to demand predictions across different forecast horizons. Minor results corresponding to RQ2 are reported in the e-companion (EC.5.5).

Finding 3: Life cycle dynamics, recent demand patterns, and operational signals are key predictors of short-term automotive demand. At short-term horizons (e.g., one month ahead), the strongest predictors of automotive demand are (i) a volume-weighted life cycle variable, indicating sensitivity to model maturity, (ii) autoregressive sales features (rolling means and exponentially weighted averages), and (iii) operational indicators such as backorders and dealer stock levels. The life cycle effect highlights that demand is lowest for newly launched models and peaks in mid-life phases, while autoregressive features confirm that short-term demand is strongly path-dependent. Operational signals provide additional explanatory power: backorders proxy unmet demand, while low dealer stocks indicate constrained supply. Interestingly, the stock price of Qualcomm (ticker symbol: QCOM), a major semiconductor supplier, emerges as an informative external predictor, reflecting supply chain dependencies. By contrast, online configurator data con-

tributes little at this horizon, consistent with its forward-looking nature and the lag between online interest and final purchase decisions (e.g., test drives, dealer negotiations, financing).

These results suggest that short-term automotive demand is primarily reactive, driven by recent momentum and immediate constraints rather than forward-looking signals. For practitioners, the implications are threefold: (i) incorporating life cycle maturity into models supports more accurate production scheduling during new model launches and end-of-life transitions, (ii) monitoring supplier-linked financial indicators can serve as early warnings of upstream supply chain disruptions, and (iii) embedding stock-related operational signals enhances dealer replenishment and reduces the risk of stockouts. These insights underscore the importance of combining internal operational data with external signals to improve short-term forecast robustness.

Finding 4: Online engagement, internal sales expectations, and evolving product life cycle feature gain relevance at longer horizons. At medium-term horizons (e.g., six months ahead), SHAP analysis reveals a distinct shift in predictor relevance compared to the short term. Internal planning targets (e.g., budget, committed orders), normalized life cycle features, and online engagement signals dominate, while the influence of weighted life cycle indicators declines. The rise of the normalized life cycle variable suggests that the model generalizes maturity effects across the portfolio, enabling inference even for early-stage or low-volume models. Online engagement data, though weak at short horizons, gains predictive power as early consumer interest gradually converts into orders. Competitive financial indicators, such as the stock performance of peer brands, show a negative influence on demand predictions, reflecting competitive pressures and potential market share shifts.

These results indicate that forecasting at longer horizons transitions from reactive signals to anticipatory drivers aligned with strategic planning. For OEMs, the implications are threefold: (i) generalized life cycle modeling enhances demand predictability for niche products, reducing reliance on sparse historical data; (ii) integrating online engagement provides early visibility into emerging consumer preferences, supporting proactive marketing and product mix optimization; and (iii) monitoring financial signals of rival brands acts as a proxy for competitive dynamics, enabling OEMs to anticipate market pressure and adapt inventory, pricing, and resource allocation accordingly. These insights highlight the value of blending internal expectations, external demand signals, and competitive intelligence in medium-term planning.

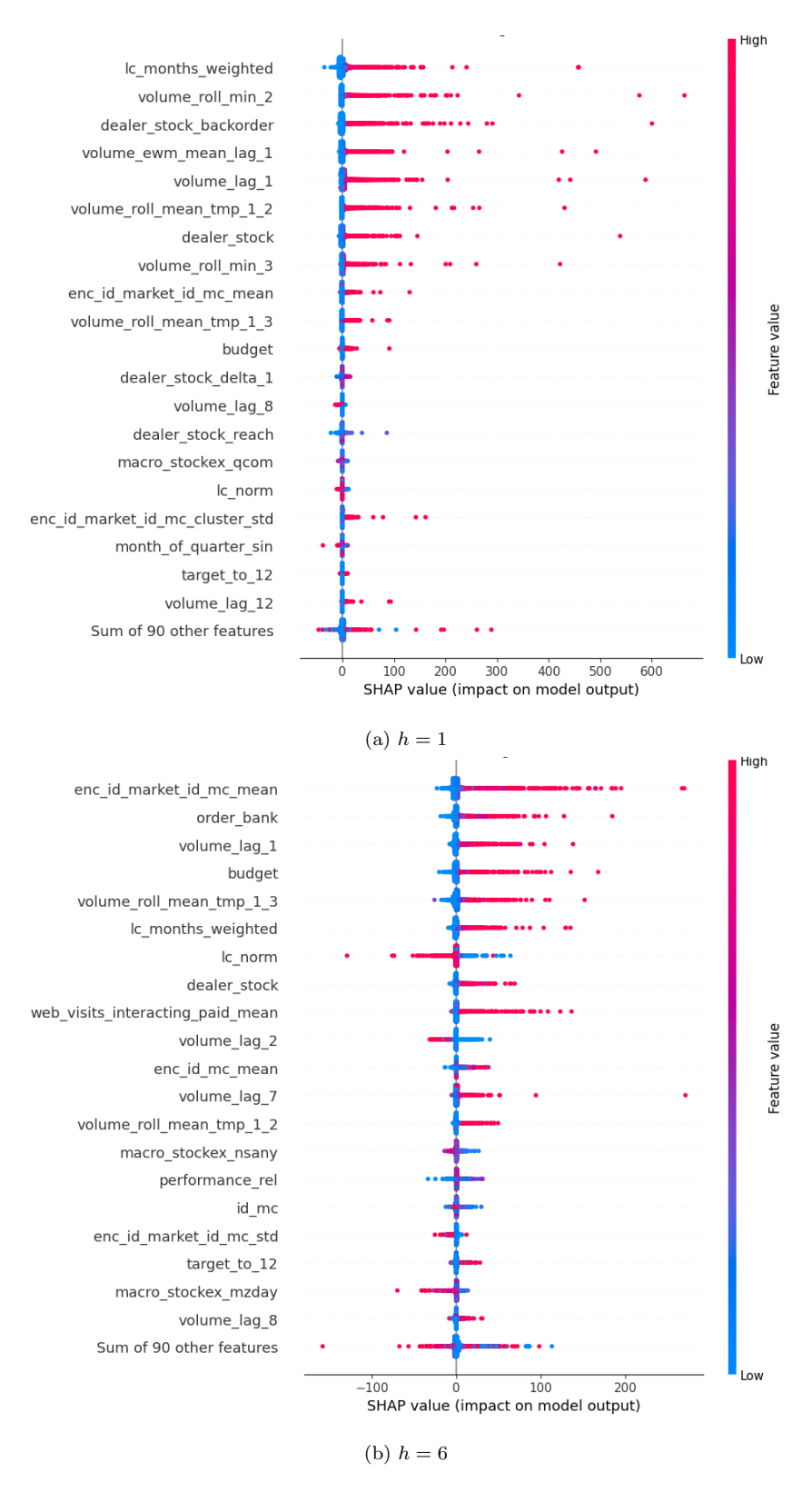


Figure 4: Distribution of SHAP values per feature for forecast steps 1 and 6.

5.3. Value of user-generated online information

To quantify the impact of user-generated online information on forecast accuracy (RQ3), we estimated linear mixed-effects models. This modeling approach captures intra-market and intraperiod dependencies arising from the rolling-horizon evaluation procedure, where overlapping test
sets introduce correlation between observations. The full specification of the mixed-effects models
and statistical tests is provided in Appendix C, and the results are summarized in Table 4.

Model	Level ID	β_0	β_1	$\hat{\sigma}_u$	$\hat{\sigma}_v$	$\hat{\sigma}$	R^2	r
LightGBM DIR	4	1.015	-0.022 [-0.044, -0.000]*	0.672	1.623	0.321	0.984	0.714***
	3	0.862	$-0.012 [-0.022, -0.002]^*$	0.489	0.887	0.093	0.996	0.495^{*}
	0-2	No sig	mificant effect detected.					
LightGBM REC	4	1.229	$-0.010 [-0.019, -0.000]^*$	0.821	3.368	0.144	0.999	0.768^{**}
	3	0.950	-0.010 [-0.016, -0.004]***	0.525	1.010	0.057	0.999	0.635^{***}
	0-2	No sig	mificant effect detected.					
DRFAM-PP (OPT)	4	0.833	-0.058 [-0.089, -0.027]***	0.602	1.389	0.407	0.965	0.121*

Table 4: Statistical test results assessing the impact of user-generated online information on forecasting error (WMAPE) across different models and hierarchical levels.

Notes. *: p < 0.05, **: p < 0.01, ***: p < 0.001.

Finding 5: User-generated online information significantly improves forecast accuracy at disaggregated levels. Across all evaluated forecasting models, the inclusion of user-generated online data significantly enhanced forecast accuracy at the most granular level (Market-Product Type). For example, in DRFAM-PP (OPT), the largest improvement was observed with a WMAPE reduction of 5.8% (p < 0.001), confirmed by non-parametric testing (Wilcoxon signed-rank test; r = 0.121, p = 0.020). Similar gains occurred in both direct and recursive LightGBM models. At the Market-Product Line level, improvements were smaller but remained statistically significant. No benefits emerged at higher aggregation levels, largely due to the limited historical span of configurator data (available from Year 9), which restricts the overlap with long-term demand series and reduces the effective training sample. Random-effects estimates revealed substantial heterogeneity across markets and forecast periods: variance components for both consistently exceeded the residual variance. This underscores that forecast performance is shaped not only by idiosyncratic noise but also by structural market differences and temporal fluctuations, echoing the spatial dependencies highlighted in Finding 1.

The predictive value of online data is strongest when it directly captures product-level demand signals, where user activity (e.g., configurator interactions or comparable digital footprints) reflects concrete purchase intentions. For premium OEMs, integrating such forward-looking, customer-centric indicators into disaggregated forecasts supports production scheduling, inventory alignment, and market allocation. In industries with high product differentiation and direct-to-consumer digital interfaces (e.g., automotive, consumer electronics, and retail), this approach enhances responsive-ness to market shifts. By contrast, at aggregated levels, online engagement data become diluted and lose predictive power, limiting their value for strategic or long-horizon projections. Similarly, generic web indicators (e.g., search-trend data) tend to capture attention at category (e.g., product line) rather than item (e.g., product type) level and are therefore only weakly related to realized demand, reducing their relevance for operational planning.

6. Conclusion

This study addressed automotive demand forecasting in a premium OEM setting by integrating hierarchical forecasting, life cycle modeling, spatiotemporal dynamics, and behavioral signals into a unified empirical framework.

(RQ1) Forecasting performance varies systematically by aggregation level: at intermediate levels, global ensemble models deliver the highest point and probabilistic accuracy, while at the most granular Market–Product Type level, pooled ensembles combining multiple forecasting strategies (DRFAM-PP) excel. This level is particularly critical for premium OEMs with high product variety, where accurate forecasts directly condition operational costs. Integer-coherent reconciliation (REC-MILP and REC-MILP-LW) further proved essential, ensuring operational feasibility by mitigating rounding biases that otherwise distort bottom-level forecasts. (RQ2) The analysis shows that forecast drivers evolve with the horizon. Short-term demand is dominated by reactive dynamics (e.g., life cycle maturity, autoregressive momentum, and operational constraints), while medium-term demand relies more on anticipatory signals such as online engagement, planning targets, and competitive financial indicators. (RQ3) User-generated online data significantly improves accuracy at disaggregated levels, highlighting its role as a forward-looking, customer-centric signal, though its predictive power diminishes at higher levels, where aggregation dilutes behavioral information. Importantly, random-effects estimates show that these gains depend on spatiotemporal differences.

Beyond these findings, we makes several generalizable methodological contributions. We extend DRFAM-PP (M5 Accuracy winner) to a stochastic pooled ensemble and generalizes pooling-set selection as a data-driven partitioning problem (POOL-SEL-BP) that trades off accuracy and model complexity. Empirically, purely hierarchical pooling is non-optimal; optimal data-driven pooling yields statistically significant accuracy gains. Integer-coherent reconciliation (REC-MILP/REC-LW-MILP) unifies empirical-risk minimization with discrete feasibility and can be extended to a wide range of hierarchical and operational forecasting settings. The proposed life-cycle feature (AVM) is shape-agnostic and transferable, supporting applications beyond the automotive domain.

For practitioners, the findings provide actionable managerial guidance: deploy resource-intensive pooled ensembles in mature, high-volume markets; rely on statistical methods in growth-phase regions; integrate online engagement data into disaggregated planning; and apply discrete reconciliation to ensure forecasts translate into feasible operational decisions. Future research should extend discrete forecast reconciliation to probabilistic settings and decision-aware objectives, exploit longer histories of behavioral data, and test the framework in other hierarchical industries.

Appendix A. Statistical benchmarks

Level	Metric	Naive	sNaive	MA(2)	MA(3)	MA(6)	MA(12)	ETS	ARIMA	Prophet
0: Brand	RMSSE	$\underline{0.640}$	1.029	0.652	0.664	0.832	0.950	0.766	0.982	1.199
	MSPL	0.361	0.612	$\underline{0.334}$	0.369	0.465	0.529	0.427	0.560	0.695
1: Market	RMSSE	0.650	0.680	0.687	0.648	0.710	0.658	0.670	0.685	0.743
	MSPL	0.372	0.400	0.379	0.369	0.432	0.380	$\underline{0.362}$	0.423	0.465
2: Market–Product Cluster	RMSSE	0.629	0.828	0.609	0.609	0.673	0.663	$\underline{0.608}$	0.631	0.785
	MSPL	0.406	0.487	0.391	0.418	0.423	0.433	0.406	$\underline{0.390}$	0.485
3: Market–Product Line	RMSSE	0.644	0.857	0.621	0.579	0.632	0.657	0.616	0.579	0.773
	MSPL	0.374	0.490	0.377	0.373	0.400	0.407	$\underline{0.362}$	0.535	0.455
4: Market–Product Type	RMSSE	0.547	0.862	0.563	0.559	0.614	0.606	0.577	0.539	0.949
	MSPL	0.321	0.460	0.336	0.341	0.477	0.388	0.346	$\underline{0.310}$	0.549

Table A.5: Point and probabilistic forecast accuracy across hierarchical levels of statistical benchmarks. Notes. Underlined values indicate the best accuracy, while bold numbers represent values that are at most 5% worse than the best.

Appendix B. Evaluation design and results for reconciliation methods

We compared REC-MILP and its level-weighted variant (REC-MILP-LW) against benchmark reconciliation methods (BU and MinT) as well as unreconciled base forecasts from ETS, ARIMA, and LightGBM REC models. The analysis was based on the first six-month test period (Year 12, Months 1–6), with forecasts generated for all hierarchy levels. For BU and MinT, reconciliation was applied to continuous base forecasts, followed by post hoc integer rounding. In contrast, REC-MILP and REC-MILP-LW directly produced integer-coherent forecasts through optimization, eliminating the need for a separate rounding step. For REC-MILP-LW, level weights (α_l) were tuned to prioritize bottom-level accuracy. Specifically, the bottom-level weight α_4 was optimized by grid search over [0.0, 1.0] in increments of 0.1, selecting the value that minimized bottom-level forecast error (RMSSE) on the validation set (Years 9–11) using four-fold cross-validation, with each fold covering six months. The resulting optimal weights were: ARIMA – 0.6, ETS – 0.8, and LightGBM REC – 0.4. All other levels were weighted equally according to $\alpha_l = (1 - \alpha_4)/4$, $\forall l = 0, ..., 3$.

Evaluation metrics included: (i) WMAPE and RMSSE across all hierarchy levels (Tables B.7 and B.8); (ii) Hodges-Lehmann estimates (HL) of the median difference in absolute errors between REC-MILP-LW and integer-rounded base forecasts at the Market-Product Type level, and \bar{d} , the mean of these differences (Table B.6); (iii) Paired Wilcoxon signed-rank test on the paired absolute error differences $d = AE_{\text{REC-MILP-LW}} - AE_{\text{Base (rounded)}}, d \neq 0$, with null hypothesis H_0 : median(d) = 0 and alternative H_1 : median(d) < 0 (i.e., REC-MILP-LW yields lower errors). We report the number of pairs (N_r), the Wilcoxon test statistic (V), the p-value (p), and the rank-biserial correlation (r_{rb}) as the effect size (Table B.6). The tests were conducted using the Python SciPy 1.16.1 library.

Method	N_r	V	p	$r_{ m rb}$	HL	\bar{d}
ETS	50	666	0.609	0.080	0.500 [-1.000 1.000]	0.040 [-1.879 1.959]
ARIMA	299	13346	3.425×10^{-12}	-0.378	-1.000 [-5.550 1.000]	-0.545 [-3.175 2.084]
LightGBM REC	84	1312	0.017	-0.333	-1.000 [-230.725 97.325]	-8.000 [-120.153 104.153]

Table B.6: Wilcoxon signed-rank test results comparing REC-MILP-LW and integer-rounded base forecasts at the Market-Product Type level.

Notes. Negative HL, \bar{d} , and $r_{\rm rb}$ values indicate that REC-MILP-LW had lower absolute errors than the rounded base forecasts.

Method	Level	Base	BU	MinT	REC-MILP	REC-MILP-LW
ETS	0: Brand	0,313	0,632	0,433	0,318	0,313
	1: Market	0,338	1,194	0,513	0,337	0,338
	2: Market–Product Cluster	0,451	1,408	0,657	0,430	0,429
	3: Market–Product Line	0,656	1,000	0,686	0,657	0,642
	4: Market–Product Type	0,600	1,538	$0,\!538$	$0,\!545$	0,529
ARIMA	0: Brand	0,269	$0,\!562$	0,396	0,258	0,317
	1: Market	0,304	0,712	0,393	0,309	0,327
	2: Market–Product Cluster	$0,\!454$	0,888	$0,\!562$	0,411	$0,\!415$
	3: Market–Product Line	0,625	0,924	0,719	0,621	0,571
	4: Market–Product Type	0,616	0,579	0,721	0,718	0,545
LightGBM REC	0: Brand	0,185	0,304	0,301	0,257	0,318
	1: Market	0,350	0,359	0,352	0,324	0,333
	2: Market–Product Cluster	0,435	$0,\!431$	$0,\!415$	0,413	0,445
	3: Market–Product Line	0,409	0,594	0,568	0,514	0,597
	4: Market–Product Type	0,566	$0,\!566$	0,666	0,619	$\underline{0,566}$

Table B.7: Accuracy of reconciliation methods (WMAPE) across the hierarchy.

Notes. Underlined values indicate the best accuracy, while bold numbers represent values that are at most 5% worse than the best. The base forecast is not included in this comparison.

Method	Level	Base	BU	MinT	REC-MILP	REC-MILP-LW
ETS	0: Brand	1,159	2,219	1,552	1,159	1,159
	1: Market	0,644	1,741	0,898	0,647	0,650
	2: Market–Product Cluster	0,605	1,535	0,846	0,649	0,650
	3: Market–Product Line	0,566	1,042	0,660	$0,\!632$	0,628
	4: Market–Product Type	0,605	0,813	0,806	0,823	0,823
ARIMA	0: Brand	1,027	1,964	1,418	0,987	1,161
	1: Market	0,628	1,253	0,710	0,648	0,657
	2: Market–Product Cluster	0,587	1,035	0,732	0,627	0,596
	3: Market–Product Line	0,507	0,752	0,595	0,607	0,605
	4: Market–Product Type	0,609	0,764	0,813	0,841	0,765
LightGBM REC	0: Brand	0,764	1,141	1,154	1,006	1,086
	1: Market	0,613	$0,\!592$	0,608	0,617	0,631
	2: Market–Product Cluster	0,643	0,644	0,603	0,606	0,654
	3: Market–Product Line	0,559	$0,\!574$	$0,\!574$	0,573	0,609
	4: Market–Product Type	0,821	0,821	0,815	0,866	0,837

Table B.8: Accuracy of reconciliation methods (RMSSE) across the hierarchy.

Notes. Underlined values indicate the best accuracy, while bold numbers represent values that are at most 5% worse than the best. The base forecast is not included in this comparison.

Appendix C. Mixed-effects model and statistical testing

To assess the impact of user-generated online information on forecast accuracy, we estimated a linear mixed-effects model of the form:

$$y_{ijk} = \beta_0 + \beta_1 \text{Online}_{ijk} + u_j + v_k + \epsilon_{ijk}, \tag{C.1}$$

where y_{ijk} denotes the forecast accuracy for time series i in market j and test period k; Online $_{ijk}$ is a binary indicator for the use of online data (1 if used, 0 otherwise); β_0 is the intercept representing the mean accuracy without online data; β_1 captures the fixed effect of including online data; $u_j \sim \mathcal{N}(0, \sigma_u^2)$ is a random effect accounting for unobserved market-level variation; $v_k \sim \mathcal{N}(0, \sigma_v^2)$ represents the random effect of test period differences; and $\epsilon_{ijk} \sim \mathcal{N}(0, \sigma^2)$ is the residual error term. Parameters were estimated using restricted maximum likelihood.

As a robustness check, we conducted the Wilcoxon signed-rank test comparing paired forecast accuracy outcomes between models with and without online data. The hypotheses were defined as: H_0 : median(d) = 0 (no accuracy difference) and alternative H_1 : median(d) < 0 (online data reduces forecast errors), where $d = WMAPE_{\text{with online}} - WMAPE_{\text{without online}}, d \neq 0$. This test was applied separately for each forecasting approach and hierarchy level. We report two key statistical measures to aid interpretation. First, the marginal R^2 , representing the proportion of variance explained by fixed effects only. Second, the standardized effect (r), derived from the Wilcoxon signed rank test, representing the effect size of the forecast accuracy differences. Values of 0.1, 0.3, and 0.5 are commonly interpreted as small, moderate, and large effects, respectively.

The analysis was based on forecast errors (WMAPE) from the test periods described in Section 4.1. Each forecasting model (LightGBM DIR, -REC, and DRFAM-PP) was evaluated with and without user-generated online features across all markets and seven rolling forecast periods, covering all hierarchy levels. These errors served as input for both the linear mixed-effects model and the Wilcoxon signed-rank test. The tests were conducted using the Python SciPy 1.16.1 library.

Declaration of Generative AI and AI-assisted technologies in the writing process

During the preparation of this work, the authors used OpenAI's ChatGPT in order to improve language clarity and readability. After using this tool, the authors reviewed and edited the content as needed and take full responsibility for the content of the publication.

References

- Aas, K., Jullum, M., & Løland, A. (2021). Explaining individual predictions when features are dependent: More accurate approximations to Shapley values. *Artificial Intelligence*, 298, 103502. doi:10.1016/j.artint.2021.103502.
- Anderer, M., & Li, F. (2022). Hierarchical forecasting with a top-down alignment of independent-level forecasts. *International Journal of Forecasting*, 38, 1405–1414. doi:10.1016/j.ijforecast.2021.12.015.
- Arora, S., Taylor, J. W., & Mak, H.-Y. (2023). Probabilistic forecasting of patient waiting times in an emergency department. *Manufacturing & Service Operations Management*, 25, 1489–1508. doi:10.1287/msom.2023.1210.
- Athanasopoulos, G., Hyndman, R. J., Kourentzes, N., & Panagiotelis, A. (2024). Fore-cast reconciliation: A review. *International Journal of Forecasting*, 40, 430–456. doi:10.1016/j.ijforecast.2023.10.010.
- Babai, M. Z., Boylan, J. E., & Rostami-Tabar, B. (2022). Demand forecasting in supply chains: A review of aggregation and hierarchical approaches. *International Journal of Production Research*, 60, 324–348. doi:10.1080/00207543.2021.2005268.
- Ben Taieb, S., Bontempi, G., Atiya, A. F., & Sorjamaa, A. (2012). A review and comparison of strategies for multi-step ahead time series forecasting based on the NN5 forecasting competition. *Expert Systems with Applications*, 39, 7067–7083. doi:10.1016/j.eswa.2012.01.039.
- Ben Taieb, S., & Koo, B. (2019). Regularized regression for hierarchical forecasting without unbiasedness conditions. In *Proceedings of the 25th ACM SIGKDD International Conference on Knowledge Discovery & Data Mining KDD '19* (p. 1337–1347). New York, NY, USA: Association for Computing Machinery. doi:10.1145/3292500.3330976.
- Berkovec, J. (1985). Forecasting automobile demand using disaggregate choice models. *Transportation Research Part B: Methodological*, 19, 315–329. doi:10.1016/0191-2615(85)90039-6.
- Bi, X., Adomavicius, G., Li, W., & Qu, A. (2022). Improving sales forecasting accuracy: A tensor

- factorization approach with demand awareness. INFORMS Journal on Computing, 34, 1644–1660. doi:10.1287/ijoc.2021.1147.
- Bottani, E., Mordonini, M., Franchi, B., & Pellegrino, M. (2021). Demand forecasting for an automotive company with neural network and ensemble classifiers approaches. In A. Dolgui, A. Bernard, D. Lemoine, G. von Cieminski, & D. Romero (Eds.), Advances in Production Management Systems. Artificial Intelligence for Sustainable and Resilient Production Systems (pp. 134–142). Cham: Springer International Publishing.
- Breiman, L. (1996). Bagging predictors. *Machine Learning*, 24, 123–140. doi:10.1023/A:1018054314350.
- Brown, G., Wyatt, J. L., & Tiňo, P. (2005). Managing diversity in regression ensembles. *Journal of Machine Learning Research*, 6, 1621–1650.
- Ding, C., & Peng, H. (2003). Minimum redundancy feature selection from microarray gene expression data. In *Computational Systems Bioinformatics*. *CSB2003*. *Proceedings of the 2003 IEEE Bioinformatics Conference*. *CSB2003* (pp. 523–528). doi:10.1109/CSB.2003.1227396.
- Ding, F., Zhu, Y., Yin, Q., Cai, Y., & Zhang, D. (2023). MS-ResCnet: A combined spatiotemporal modeling and multi-scale fusion network for taxi demand prediction. *Computers and Electrical Engineering*, 105, 108558. doi:10.1016/j.compeleceng.2022.108558.
- Du, R. Y., Hu, Y., & Damangir, S. (2015). Leveraging trends in online searches for product features in market response modeling. *Journal of Marketing*, 79, 29–43. doi:10.1509/jm.12.0459.
- Elalem, Y. K., Maier, S., & Seifert, R. W. (2023). A machine learning-based framework for fore-casting sales of new products with short life cycles using deep neural networks. *International Journal of Forecasting*, 39, 1874–1894. doi:10.1016/j.ijforecast.2022.09.005.
- Fantazzini, D., & Toktamysova, Z. (2015). Forecasting German car sales using Google data and multivariate models. *International Journal of Production Economics*, 170, 97–135. doi:10.1016/j.ijpe.2015.09.010.
- Gammelli, D., Wang, Y., Prak, D., Rodrigues, F., Minner, S., & Pereira, F. C. (2022). Predictive

- and prescriptive performance of bike-sharing demand forecasts for inventory management. *Transportation Research Part C: Emerging Technologies*, 138, 103571. doi:10.1016/j.trc.2022.103571.
- Geng, N., Jiang, Z., & Chen, F. (2009). Stochastic programming based capacity planning for semiconductor wafer fab with uncertain demand and capacity. European Journal of Operational Research, 198, 899–908. doi:10.1016/j.ejor.2008.09.029.
- Georgiadis, P., Vlachos, D., & Tagaras, G. (2006). The impact of product lifecycle on capacity planning of closed-loop supply chains with remanufacturing. *Production and Operations Management*, 15, 514–527. doi:10.1111/j.1937-5956.2006.tb00160.x.
- Gonçalves, J. N., Cortez, P., Carvalho, M. S., & Frazão, N. M. (2021). A multivariate approach for multi-step demand forecasting in assembly industries: Empirical evidence from an automotive supply chain. *Decision Support Systems*, 142, 113452. doi:10.1016/j.dss.2020.113452.
- Guo, X., Grushka-Cockayne, Y., & De Reyck, B. (2021). Forecasting airport transfer passenger flow using real-time data and machine learning. *Manufacturing & Service Operations Management*, 24, 3193–3214. doi:10.1287/msom.2021.0975.
- Guo, X., Lichtendahl, K. C., & Grushka-Cockayne, Y. (2024). Bayesian ensembles of exponentially smoothed life-cycle forecasts. *Manufacturing & Service Operations Management*, 27. doi:10.1287/msom.2022.0359.
- Guo, Y., Zhang, Y., Boulaksil, Y., & Tian, N. (2022). Multi-dimensional spatiotemporal demand forecasting and service vehicle dispatching for online car-hailing platforms. *International Journal* of Production Research, 60, 1832–1853. doi:10.1080/00207543.2021.1871675.
- Hollyman, R., Petropoulos, F., & Tipping, M. E. (2021). Understanding forecast reconciliation. European Journal of Operational Research, 294, 149–160. doi:10.1016/j.ejor.2021.01.017.
- Hu, K., Acimovic, J., Erize, F., Thomas, D. J., & Van Mieghem, J. A. (2018). Forecasting new product life cycle curves: Practical approach and empirical analysis. *Manufacturing & Service Operations Management*, 21, 66–85. doi:10.1287/msom.2017.0691.
- Hyndman, R. J., Ahmed, R. A., Athanasopoulos, G., & Shang, H. L. (2011). Optimal combination

- forecasts for hierarchical time series. Computational Statistics & Data Analysis, 55, 2579–2589. doi:10.1016/j.csda.2011.03.006.
- Hyndman, R. J., Lee, A. J., & Wang, E. (2016). Fast computation of reconciled forecasts for hierarchical and grouped time series. *Computational Statistics & Data Analysis*, 97, 16–32. doi:10.1016/j.csda.2015.11.007.
- In, Y., & Jung, J.-Y. (2022). Simple averaging of direct and recursive forecasts via partial pooling using machine learning. *International Journal of Forecasting*, 38, 1386–1399. doi:10.1016/j.ijforecast.2021.11.007.
- Ke, G., Meng, Q., Finley, T., Wang, T., Chen, W., Ma, W., Ye, Q., & Liu, T.-Y. (2017). Light-GBM: A highly efficient gradient boosting decision tree. In I. Guyon, U. V. Luxburg, S. Bengio, H. Wallach, R. Fergus, S. Vishwanathan, & R. Garnett (Eds.), Advances in Neural Information Processing Systems. Curran Associates, Inc. volume 30.
- Kurawarwala, A. A., & Matsuo, H. (1996). Forecasting and inventory management of short life-cycle products. *Operations Research*, 44, 131–150. doi:10.1287/opre.44.1.131.
- Lainder, A. D., & Wolfinger, R. D. (2022). Forecasting with gradient boosted trees: augmentation, tuning, and cross-validation strategies: Winning solution to the M5 uncertainty competition. *International Journal of Forecasting*, 38, 1426–1433. doi:10.1016/j.ijforecast.2021.12.003.
- Li, Y., Sun, H., Lv, Y., & Chang, X. (2024). Ridesplitting demand prediction via spatiotemporal multi-graph convolutional network. Expert Systems with Applications, 247, 123207. doi:10.1016/j.eswa.2024.123207.
- Liang, Y., Ke, S., Zhang, J., Yi, X., & Zheng, Y. (2018). GeoMAN: Multi-level attention networks for geo-sensory time series prediction. In *Proceedings of the 27th International Joint Conference on Artificial Intelligence* (pp. 3428–3434). International Joint Conferences on Artificial Intelligence Organization. doi:10.24963/ijcai.2018/476.
- Lotfi, A., Jiang, Z., Lotfi, A., & Jain, D. C. (2022). Estimating life cycle sales of technology products with frequent repeat purchases: A fractional calculus-based approach. *Information Systems Research*, 34, 409–422. doi:10.1287/isre.2022.1131.

- Lundberg, S. M., & Lee, S.-I. (2017). A unified approach to interpreting model predictions. In I. Guyon, U. V. Luxburg, S. Bengio, H. Wallach, R. Fergus, S. Vishwanathan, & R. Garnett (Eds.), Advances in Neural Information Processing Systems. Curran Associates, Inc. volume 30.
- Makridakis, S., Spiliotis, E., & Assimakopoulos, V. (2022a). M5 accuracy competition: Results, findings, and conclusions. *International Journal of Forecasting*, 38, 1346–1364. doi:10.1016/j.ijforecast.2021.11.013.
- Makridakis, S., Spiliotis, E., Assimakopoulos, V., Chen, Z., Gaba, A., Tsetlin, I., & Winkler, R. L. (2022b). The M5 uncertainty competition: Results, findings and conclusions. *International Journal of Forecasting*, 38, 1365–1385. doi:10.1016/j.ijforecast.2021.10.009.
- Montero-Manso, P., & Hyndman, R. J. (2021). Principles and algorithms for forecasting groups of time series: Locality and globality. *International Journal of Forecasting*, 37, 1632–1653. doi:10.1016/j.ijforecast.2021.03.004.
- Moreno, A., & Terwiesch, C. (2016). The effects of product line breadth: Evidence from the automotive industry. *Marketing Science*, 36, 254–271. doi:10.1287/mksc.2016.0979.
- Olivares, K. G., Challu, C., Marcjasz, G., Weron, R., & Dubrawski, A. (2023). Neural basis expansion analysis with exogenous variables: Forecasting electricity prices with NBEATSx. *International Journal of Forecasting*, 39, 884–900. doi:10.1016/j.ijforecast.2022.03.001.
- Onyeocha, C. E., Khoury, J., & Geraghty, J. (2015). Evaluation of multi-product lean manufacturing systems with setup and erratic demand. *Computers & Industrial Engineering*, 87, 465–480. doi:10.1016/j.cie.2015.05.029.
- Panagiotelis, A., Athanasopoulos, G., Gamakumara, P., & Hyndman, R. J. (2021). Forecast reconciliation: A geometric view with new insights on bias correction. *International Journal of Forecasting*, 37, 343–359. doi:10.1016/j.ijforecast.2020.06.004.
- Salari, N., Liu, S., & Shen, Z.-J. M. (2022). Real-time delivery time forecasting and promising in online retailing: When will your package arrive? *Manufacturing & Service Operations Management*, 24, 1421–1436. doi:10.1287/msom.2022.1081.

- Salinas, D., Flunkert, V., Gasthaus, J., & Januschowski, T. (2020). DeepAR: Probabilistic forecasting with autoregressive recurrent networks. *International Journal of Forecasting*, 36, 1181–1191. doi:10.1016/j.ijforecast.2019.07.001.
- Schaer, O., Kourentzes, N., & Fildes, R. (2019). Demand forecasting with user-generated online information. *International Journal of Forecasting*, 35, 197–212. doi:10.1016/j.ijforecast.2018.03.005.
- Staeblein, T., & Aoki, K. (2015). Planning and scheduling in the automotive industry: A comparison of industrial practice at german and japanese makers. *International Journal of Production Economics*, 162, 258–272. doi:10.1016/j.ijpe.2014.07.005.
- Syntetos, A. A., Boylan, J. E., & Croston, J. D. (2005). On the categorization of demand patterns.

 Journal of the Operational Research Society, 56, 495–503. doi:10.1057/palgrave.jors.2601841.
- Taylor, S. J., & Letham, B. (2018). Forecasting at scale. *The American Statistician*, 72, 37–45. doi:10.1080/00031305.2017.1380080.
- Wickramasuriya, S. L., Athanasopoulos, G., & Hyndman, R. J. (2019). Optimal forecast reconciliation for hierarchical and grouped time series through trace minimization. *Journal of the American Statistical Association*, 114, 804–819. doi:10.1080/01621459.2018.1448825.
- Wickramasuriya, S. L., Turlach, B. A., & Hyndman, R. J. (2020). Optimal non-negative forecast reconciliation. *Statistics and Computing*, 30, 1167–1182. doi:10.1007/s11222-020-09930-0.
- Yao, X., Shen, X., He, T., & Son, S. H. (2018). Demand estimation of public bike-sharing system based on temporal and spatial correlation. In 4th International Conference on Big Data Computing and Communications (BIGCOM) (pp. 60–65). doi:10.1109/BIGCOM.2018.00016.
- Zhang, B., Panagiotelis, A., & Kang, Y. (2024). Discrete forecast reconciliation. *European Journal of Operational Research*, 318, 143–153. doi:10.1016/j.ejor.2024.05.024.
- Zhang, C., Tian, Y.-X., & Fan, Z.-P. (2022). Forecasting sales using online review and search engine data: A method based on PCA-DSFOA-BPNN. *International Journal of Forecasting*, 38, 1005–1024. doi:10.1016/j.ijforecast.2021.07.010.

Electronic companion

Automobile demand forecasting: Spatiotemporal and hierarchical modeling, life cycle dynamics, and user-generated online information

Tom Nahrendorf, Stefan Minner, Helfried Binder, Richard Zinck

EC.1. Computation details

All computations were performed on a system with an Intel Core i7 processor (6 cores, 2.6 GHz) and 16 GB of RAM, running macOS Sonoma 14.7.3. The analysis was conducted in Python 3.11.10 using the following libraries: scikit-learn 1.5.2 for direct (DIR) and hybrid (HYB) forecasting strategies and data pipelining; MLForecast 1.0.2 (Nixtla) for recursive (REC) forecasting; NeuralForecast 3.0.0 for deep learning models (DeepAR, NBEATSx); HierarchicalForecast 1.2.1 for hierarchical reconciliation benchmarks; and the Gurobi Optimizer 12.0.1 for solving the proposed pooling selection model (POOL-SEL-BP), and mixed-integer linear programming reconciliation models (REC-MILP and REC-MILP-LW).

EC.2. Market clustering

Market clustering was introduced to reduce heterogeneity in demand dynamics across markets and to enable more homogeneous model training. Total market volumes were used in raw form, with no missing values detected. A total of 783 time-series features were extracted with the *tsfresh* library (default settings), and all features were standardized prior to dimensionality reduction. Principal component analysis (*scikit-learn*, default settings) reduced the feature space to 16 components, explaining 95% of the variance. Standard k-means clustering (*scikit-learn*, k-means++ initialization, objective: intra-cluster variance) was applied, with five clusters selected using the elbow method based on inertia and cluster size balance. This avoided degenerate solutions with many small clusters. The resulting clusters comprised 2, 9, 1, 1, and 10 markets, respectively, covering all 23 markets.

For robustness, we evaluated clustering based on dynamic time warping (DTW). However, DTW-based clustering resulted in higher forecast bias in the test period (Year 12). Using a Light-GBM model trained separately per cluster, the forecast bias was 6,056 for feature-based clustering, 11,501 for DTW clustering, and 11,510 for a global model without clustering.

EC.3. Pooling set selection

Table EC.1 summarizes the candidate pooling families \mathcal{G} considered in POOL-SEL-BP. Each pool g represents a feasible partition of training data; the reported quantities describe its structural and cost characteristics. The pool size M_q denotes the number of models trained under that

grouping, and G_g is the Gini coefficient of the within-pool series sample-share distribution (higher = more imbalance). The no-pooling baseline, representing local models trained individually per series (naive forecast), was included with $\kappa_{\text{no pooling}} = 0$ to provide a zero-cost fallback and guarantee feasibility. In total, ten candidate pools plus no-pooling were evaluated (hierarchical, domain-based, clustering-based, and combined forms). Other candidate combinations (e.g., Market-Product Line, implying $23 \times 17 = 391$ models for each direct and recursive learner) were considered but deemed non-feasible by the industry partner due to excessive model-training complexity.

Pool g	Pool size (M_g)	Sample imbalance (G_g)	Pool cost (κ_g)
Hierarchical			
Market	23	0.1267	0.0148
Product Cluster	5	0.1807	0.0092
Product Line	14	0.4666	0.0243
Market–Product Cluster	92	0.2409	0.0487
$Domain\mbox{-}based$			
Market maturity	2	0.1900	0.0083
Fuel type	3	0.6346	0.0262
Body type	8	0.3115	0.0156
$Clustering ext{-}based$			
Market cluster*	5	0.4146	0.0184
Combinations			
Market cluster–fuel type	15	0.7753	0.0368
Market cluster-body type	40	0.5255	0.0377

Table EC.1: Candidate pooling families and associated costs.

Notes. *: For specification of the market clustering procedure, see e-companion EC.2.

To capture both computational complexity and risk of overfitting, we defined the pool cost as $\kappa_g = sM_g(1 + \nu G_g)$, where the scale factor s aligns the cost magnitude with the average validation loss and $\nu \geq 0$ controls the penalty for imbalance. We set $\nu = 1$ for an equal trade-off between model count and imbalance and chose $s \approx 0.0002$ so that the mean of κ_g matched the mean relative loss, giving λ an interpretable accuracy–complexity trade-off (a one-unit change in λ roughly trades one average series-level improvement against opening one additional pool). The optimization used relative losses $\Delta L_{ig} = L_{ig} - L_{i0}$ based on RMSSE, where L_{ig} is the per-fold mean of direct and recursive model losses, subsequently averaged across 12 rolling validation folds; L_{i0} denotes the

corresponding no-pooling baseline.

To calibrate the trade-off parameter λ , we solved POOL-SEL-BP for a grid of ten candidate values and recorded both the average relative validation loss and the number of pools activated. Figure EC.1 shows the resulting accuracy–complexity frontier. Each point represents the mean relative RMSSE (improvement over the local baseline) achieved for a given λ , plotted against the corresponding number of open pools. The curve is monotonically decreasing with a clear elbow at $\lambda = 35$, beyond which additional pools yield diminishing returns. We therefore set $\lambda = 35$, which opens five pools. At comparable model budgets, optimal pooling under POOL-SEL-BP outperforms fixed hierarchical pooling, confirming gains from endogenously selecting pooling structures based on validation performance.

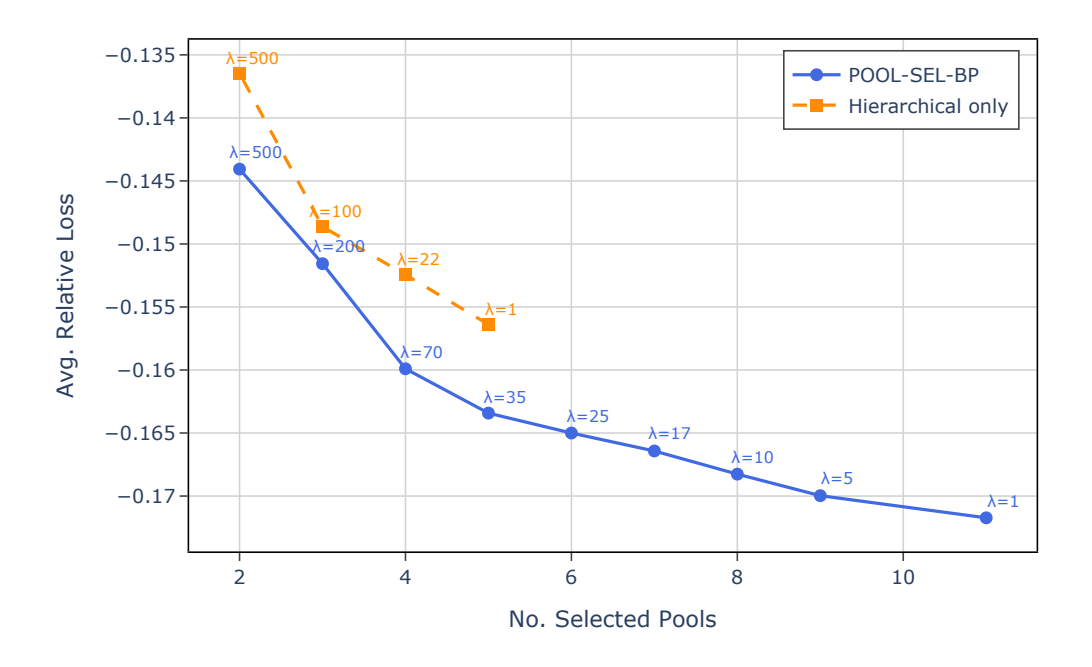


Figure EC.1: POOL-SEL-BP hyperparameter tuning.

Table EC.2 reports the optimal solution of POOL-SEL-BP. It identified four dominant pooling structures based on their cumulative improvement in relative RMSSE over the no-pooling baseline. For subsequent forecasting experiments, we selected the top three pools (body type, market, and

market cluster) as input configurations for DRFAM-PP.

Pool g	n assigned	Sum of rel. pool losses	Avg. rel. pool loss
Body type	114	-37.1718	-0.3260
Market	64	-20.3019	-0.3172
Market cluster	46	-18.4399	-0.4008
Market maturity	91	-17.8540	-0.1962

Table EC.2: Results pool selection optimization.

Body-type pooling captures structural demand heterogeneity across vehicle segments, which reflect distinct usage patterns, life cycle dynamics, and price positioning (e.g., compact vs. SUV). Market-level pooling leverages country-specific macro and regulatory conditions that shape local sales trajectories. Market-cluster pooling extends this logic by grouping markets with similar seasonal behavior, trend, and volatility patterns, enabling transfer of information across comparable regions.

EC.4. Geometry of reconciliation

We illustrate reconciliation in the minimal three-series hierarchy with two bottom series and their aggregate. Let y_1 and y_2 denote bottom-level series and y_3 the aggregate, subject to the coherence constraint $y_3 = y_1 + y_2$. In Figure EC.2, the coherent subspace $\mathcal{C} = \{a \mathbf{v}_1 + b \mathbf{v}_2 : a, b \in [0,1]\}$ appears as a parallelogram spanned by $\mathbf{v}_1 = (9,0,9)^{\top}$ and $\mathbf{v}_2 = (0,9,9)^{\top}$. We take the base (incoherent) forecast $\mathbf{P} = (1.5,5.6,8.7)^{\top}$, so $y_1 + y_2 = 7.1 \neq y_3$. Each reconciler maps \mathbf{P} to the closest coherent point in \mathcal{C} , where "closest" is defined by its metric:

- 1. OLS (identity metric, L_2 -norm): orthogonal (Euclidean) projection onto \mathcal{C} gives $\tilde{\mathbf{y}}_{\text{OLS}} = (2.033, 6.133, 8.167)^{\top}$.
- 2. MinT (weighted, L_2 -norm): projection under metric \mathbf{W} . We use MinT-shrink constructed from an illustrative forecast-error covariance $\mathbf{\Sigma} = \begin{bmatrix} 4.0 & 1.8 & 5.8 \\ 1.8 & 9.0 & 10.8 \\ 5.8 & 10.8 & 16.6 \end{bmatrix}$, $\mathbf{W} = ((1 \lambda)\mathbf{\Sigma} + \lambda \operatorname{diag}(\mathbf{\Sigma}))^{-1}$, $\lambda = 0.3$, yielding $\tilde{\mathbf{y}}_{\text{MinT}} = (1.716, 6.086, 7.803)^{\top}$.
- 3. REC-MILP (integer, L_1 -norm): L_1 projection restricted to the integer-coherent lattice $\mathcal{C} \cap \mathbb{Z}^3$ (green points) gives $\tilde{\mathbf{y}}_{\text{REC-MILP}} = (2, 6, 8)^{\top}$.

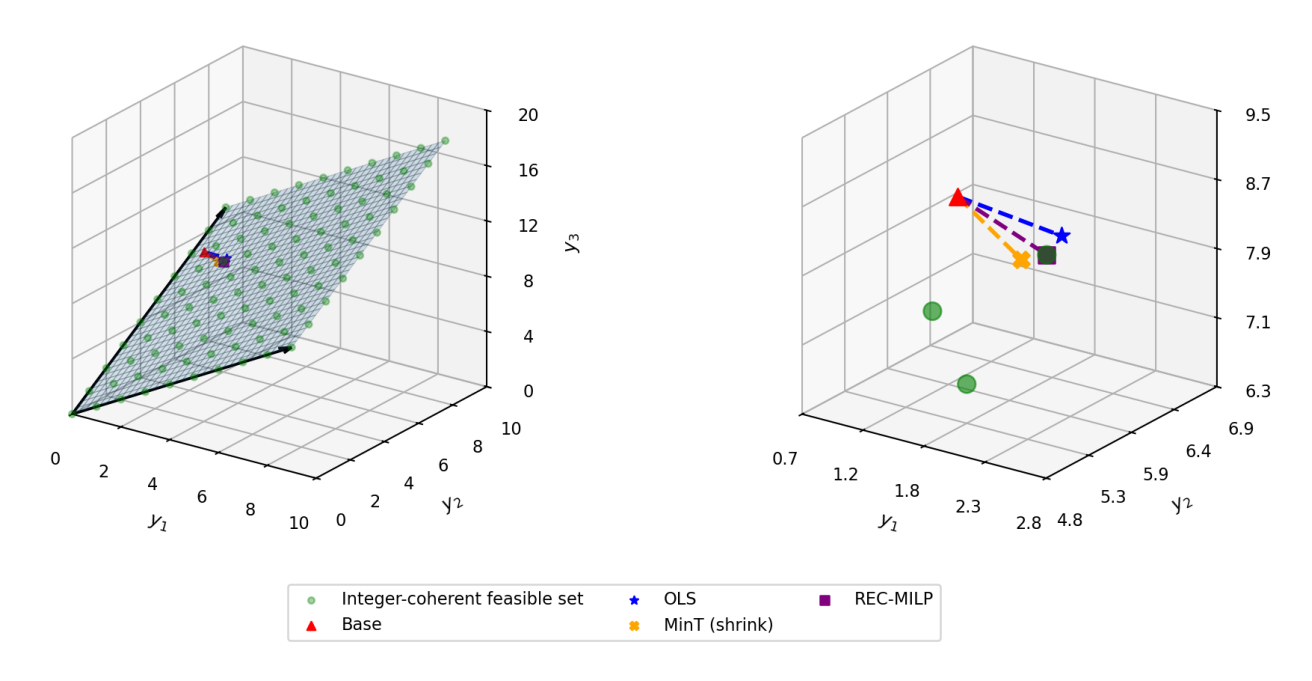


Figure EC.2: Geometry of reconciliation.

EC.5. Minor empirical results

EC.5.1. No single forecasting method is optimal across hierarchy levels

Our results confirm that no single forecasting method dominates at all hierarchical levels. Demand dynamics differ substantially between strategic levels (e.g., brand or market) and operational levels (e.g., product type). This implies that level-specific forecasting strategies are necessary to match the volatility, data richness, and planning horizon of each level. For automotive original equipment manufacturers (OEMs), this supports the adoption of hierarchical modeling frameworks, where methods are tailored to both aggregated and disaggregated decision contexts.

EC.5.2. Forecast accuracy decreases with increasing granularity

Forecast accuracy, measured in weighted mean absolute percentage error (WMAPE), decreases as the level of granularity increases, as WMAPE is directly comparable across hierarchical levels, whereas root mean squared scaled error (RMSSE) is scale-dependent and not invariant across aggregation levels. Aggregated levels (brand, market) achieve the highest accuracy, while forecasts at the product line and product type levels show higher volatility (Table EC.5.6). This finding highlights the need for OEMs to anticipate higher uncertainty in granular demand forecasts and

to incorporate probabilistic forecasts into operational planning, particularly for production and inventory allocation at the product type level.

EC.5.3. Hybrid direct-recursive forecasting improves bottom-level accuracy

At the most granular level (Market–Product Type), HYB outperforms pure DIR and REC approaches as well as deep learning models by combining DIR and REC methods through chained forecasting (Table EC.5.6). This approach leverages the horizon-specific accuracy of DIR forecasts alongside the temporal consistency of REC models, which incorporate information from previous predictions to maintain coherence across time steps. While HYB strategies did not outperform at higher levels of the hierarchy, they proved especially effective for operational-level forecasting by delivering stable and consistent planning inputs.

EC.5.4. Probabilistic forecasting at the bottom level

At the lowest hierarchy level, the Direct Recursive Forecast Averaging Method via Partial Pooling (DRFAM-PP) consistently outperforms other models across most quantiles (see EC.6.6, Figure EC.6), delivering robust probabilistic forecasts. Its performance is strongest at lower and mid quantiles, while at the upper quantiles (e.g., q = 0.975, 0.995), simple statistical benchmarks such as Naive and ARIMA slightly outperform it due to their inherent overestimation bias (see EC.6.5, Figure EC.5). In contrast, tree-based global models (LightGBM DIR, -REC, and -HYB) perform well at lower quantiles but show declining accuracy for quantiles above $q \ge 0.75$, particularly when using DIR. This underperformance is largely attributed to the lack of temporal smoothing and the inability to capture sequential dependencies in DIR models. For instance, DeepAR maintains better performance in these high quantiles by leveraging recurrent structures to model time-dependent patterns.

EC.5.5. Pricing features as locally influential predictors

Although price-related features did not surface prominently in the global SHAP analysis, local interpretability plots (Figure EC.3) show that they can strongly affect individual predictions. Aligned with economic theory, lower product prices (price_net_norm) increase predicted demand. However, a low relative price compared to the series cluster average (price_rel_cluster) can lead to lower predicted demand. This reflects perceived value dynamics: in premium markets, products priced well below peers signal lower quality, decreasing demand.

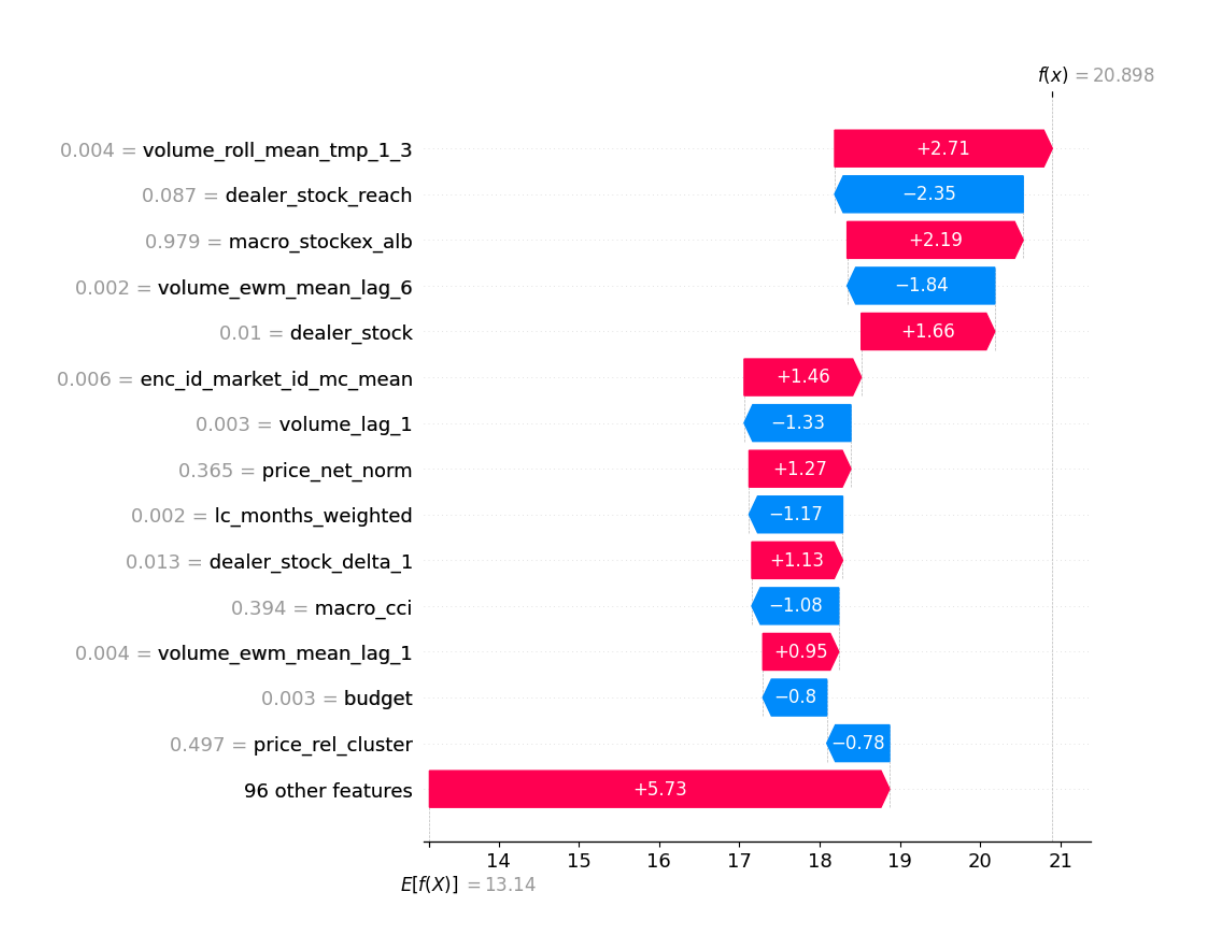


Figure EC.3: SHAP waterfall plot for forecast step 2, providing a local explanation for a specific market-product type combination.

EC.5.6. Point and probabilistic forecast accuracy across hierarchical levels

Model	RMSS	E					WMA	PE [x	100%]				Forecas	st bias	(scaled)				MSPI					
	Level	ID				Avg.	Level	ID				Avg.	Level I	D	Avg. Level ID				Avg.					
	0	1	2	3	4		0	1	2	3	4	-	0	1	2	3	4		0	1	2	3	4	_
Statistical																								
Naive	0.640	0.650	0.629	0.644	0.547	0.622	0.156	0.351	0.545	0.746	1.265	0.613	-0.103	-0.089	-0.092	-0.385	-0.241	-0.182	0.361	0.372	0.406	0.374	0.321	0.367
sNaive	1.029	0.680	0.828	0.857	0.862	0.851	0.265	0.397	0.711	0.963	1.082	0.684	-0.265	-0.273	-0.347	-0.581	-0.592	-0.412	0.612	0.400	0.487	0.490	0.460	0.490
MA(2)	0.652	0.687	0.609	0.621	0.563	0.626	0.149	0.382	0.543	0.722	0.847	0.529	-0.109	-0.167	-0.130	-0.464	-0.317	-0.237	0.334	0.379	0.391	0.377	0.336	0.363
MA(3)	0.664	0.648	0.609	0.579	0.559	0.612	0.165	0.376	0.518	0.667	0.868	0.519	-0.115	-0.132	-0.154	-0.358	-0.343	-0.220	0.369	0.369	0.418	0.373	0.341	0.374
MA(6)	0.832	0.710	0.673	0.632	0.614	0.692	0.201	0.362	0.539	0.764	0.961	0.565	-0.183	-0.226	-0.249	-0.543	-0.500	-0.340	0.465	0.432	0.423	0.400	0.477	0.419
MA(12)	0.950	0.658	0.663	0.657	0.606	0.707	0.229	0.343	0.538	0.771	1.056	0.587	-0.224	-0.244	-0.272	-0.673	-0.781	-0.439	0.529	0.380	0.433	0.407	0.388	0.427
ETS	0.766	0.670	0.608	0.616	0.577	0.647	0.185	0.365	0.506	0.746	1.265	0.613	-0.158	-0.209	-0.194	-0.581	-0.976	-0.423	0.427	0.362	0.406	0.362	0.346	0.381
ARIMA	0.982	0.685	0.631	0.579	0.539	0.683	0.250	0.384	0.498	0.709	1.000	0.568	-0.235	-0.235	-0.176	-0.375	-0.311	-0.313	0.560	0.423	0.390	0.535	0.310	0.407
Prophet	1.199	0.743	0.785	0.773	0.949	0.890	0.304	0.497	0.650	1.055	1.797	0.861	-0.304	-0.385	-0.383	-0.942	-1.520	0.703	0.695	0.465	0.485	0.455	0.549	0.530
ML-based																								
DeepAR	†	†	†	†	0.494	†	†	†	†	†	0.935	†	†	†	†	†	-0.378	†	†	†	†	†	0.182	†
NBEATSx	†	†	†	†	0.531	†	†	†	†	†	1.000	†	†	†	†	†	-0.429	†	†	†	†	†	0.654	†
LightGBM DIR	1.145	0.606	0.621	0.521	0.581	0.695	0.246	0.347	0.496	0.639	0.731	0.492	-0.257	-0.117	-0.053	-0.226	-0.192	-0.169	0.320	0.249	0.229	0.185	0.227	0.242
LightGBM REC	0.750	0.638	0.618	0.543	0.576	0.625	0.170	0.350	0.504	0.600	0.742	0.473	-0.134	-0.265	-0.108	-0.304	-0.179	-0.198	0.233	0.202	0.206	0.155	0.171	0.193
LightGBM HYB	1.267	0.730	0.804	0.675	0.478	0.791	0.306	0.387	0.700	0.835	0.677	0.581	-0.300	0.041	0.649	0.822	0.469	0.336	0.292	0.217	0.257	0.206	0.154	0.225
LightGBM ENS	1.020	0.579	0.546	0.436	0.516	0.619	0.250	0.303	0.471	0.518	0.654	0.439	-0.229	-0.094	0.143	0.086	0.026	-0.014	0.240	0.206	0.200	0.145	0.181	0.194
DRFAM-PP (HIER)	†	†	†	†	0.469	†	†	†	†	†	0.654	†	†	†	†	†	0.348	†	†	†	†	†	0.134	l †
DRFAM-PP (OPT)	†	†	†	†	0.418	†	†	†	†	†	0.695	†	†	†	†	†	0.500	†	†	†	†	†	0.128	3 †

Table EC.3: Accuracy of the base forecast over seven test periods by benchmark model and level.

Notes. \dagger : Insufficient data available for the application of the specified model. Underlined values indicate the best accuracy, while bold numbers represent values that are at most 5% worse than the best.

EC.6. Additional plots and tables

EC.6.1. Macroeconomic and financial data

Indicator	Unit	Data source
Macroeconomic		
Unemployment rate	%	Eurostat: ei_lmhr_m
Inflation rate	%	Eurostat: prc_hicp_manr
Interest rate	%	Eurostat: irt_lt_mcby_m
Exchange rate	National currency/ EUR	Eurostat: ert_bil_eur_m
GDP	Million EUR	Eurostat: namq_10_gdp
Harmonized consumer price index		
All items	Index $(2015 = 100)$	Eurostat: $prc_hicp_midx/CP00$
New vehicles	Index $(2015 = 100)$	Eurostat: prc_hicp_midx/CP07111
Personal transport equipment – Parts	Index $(2015 = 100)$	Eurostat: $prc_hicp_midx/CP0721$
Personal transport equipment – Maintenance	Index $(2015 = 100)$	Eurostat: $prc_hicp_midx/CP0723$
Personal transport equipment – Other services	Index $(2015 = 100)$	Eurostat: prc_hicp_midx/CP0724
Personal transport insurance	Index $(2015 = 100)$	Eurostat: prc_hicp_midx/CP1254
Public transport	Index (2015 = 100)	Eurostat: prc_hicp_midx/CP073
Electricity	Index $(2015 = 100)$	Eurostat: prc_hicp_midx/CP0451
Diesel	Index $(2015 = 100)$	Eurostat: prc_hicp_midx/CP07221
Petrol	$Index\ (2015 = 100)$	Eurostat: prc_hicp_midx/CP07222
Financial market		
Automotive manufacturers		
BMW AG	EUR	Yahoo Finance: BMW.DE
Mercedes-Benz Group AG	EUR	Yahoo Finance: MBG.DE
Volkswagen AG	EUR	Yahoo Finance: VOW3.DE
Tesla Inc.	USD	Yahoo Finance: TSLA
Toyota Motor Corporation	USD	Yahoo Finance: TM
Nissan Motor Co., Ltd.	USD	Yahoo Finance: NSANY
Honda Motor Co., Ltd.	USD	Yahoo Finance: HMC
Ford Motor Company	USD	Yahoo Finance: F
Stellantis N.V.	USD	Yahoo Finance: STLA
Mazda Motor Corporation	USD	Yahoo Finance: MZDAY
Supplier		
Continental AG (Parts)	EUR	Yahoo Finance: CON.DE
Aptiv PLC (Electronics)	USD	Yahoo Finance: APTV
Alcoa Corporation (Aluminium)	USD	Yahoo Finance: AA
Nucor Corporation (Steel)	USD	Yahoo Finance: NUE
Albemarle Corporation (Batteries)	USD	Yahoo Finance: ALB
QUALCOMM Incorporated (Semiconductors)	USD	Yahoo Finance: QCOM

Table EC.4: Macroeconomic and financial indicators used as explanatory variables.

Notes. The data extraction period spans 12 years, from Year 1 to Year 12, where available. Data were collected for 23 markets, but country names are withheld due to confidentiality agreements. All data are reported at monthly frequency, except for gross domestic product (GDP), which is published quarterly.

EC.6.2. Selected features by hierarchy level

Feature	Level	ID						
	0	1	2	3	4			
Demand								
Lags 1-12	○ ● ●	○ •	$\circ \bullet \bullet$	$\circ \bullet \bullet$	○ •			
Rolling minimum/maximum (windows: 1,3,6)	○ •	○ •	$\circ \bullet \bullet$	$\circ \bullet \bullet$	○ •			
Rolling sum (windows: 2,3,12)	○ •	○ •	$\circ \bullet \bullet$	$\circ \bullet \bullet$	○ •			
Rolling standard deviation (windows: 3)	$\circ \bullet \bullet$	$\circ \bullet \bullet$	$\circ \bullet \bullet$	$\circ \bullet \bullet$	○ ● ●			
Shifted rolling mean (windows: 3, shifts: 1,2,3,4)	$\circ \bullet \bullet$	$\circ \bullet \bullet$	$\circ \bullet \bullet$	$\circ \bullet \bullet$	○ •			
Exponential weighted smoothing (lags: 1,6,12)	$\circ \bullet \bullet$	$\circ \bullet \bullet$	$\circ \bullet \bullet$	$\circ \bullet \bullet$	○ •			
${\it Historic\ mean/standard\ deviation\ of\ demand\ by\ market-product\ type}$					○ •			
Historic mean/standard deviation of demand by product type					○ •			
Temporal								
Binary encoding of year/quarter	$\circ \bullet \bullet$	$\circ \bullet \bullet$	$\circ \bullet \bullet$	$\circ \bullet \bullet$	○ •			
Sinusoidal transformation of month/month of quarter	$\circ \bullet \bullet$	$\circ \bullet \bullet$	$\circ \bullet \bullet$	$\circ \bullet \bullet$	○ •			
Life cycle								
Normalized life cycle age			$\circ \bullet \bullet$	$\circ \bullet \bullet$	○ •			
Volume-weighted life cycle age			$\circ \bullet$	$\circ \bullet$	0			
Master								
Cylinder			$\circ \bullet \bullet$	$\circ \bullet \bullet$	○ •			
Doors			$\circ \bullet \bullet$	$\circ \bullet \bullet$	○ •			
Relative performance			$\circ \bullet \bullet$	$\circ \bullet \bullet$	○ •			
Product type ID					○ •			
Body type					○ •			
Fuel type					○ •			
Market cluster		$\circ \bullet \bullet$	$\circ \bullet \bullet$	$\circ \bullet \bullet$	○ •			
Market maturity		$\circ \bullet \bullet$	$\circ \bullet \bullet$	$\circ \bullet \bullet$	00•			
Internal								
Dealer inventory	$\circ \bullet$	$\circ \bullet$	$\circ \bullet$	○ •	0 0			
Dealer backorders	$\circ \bullet$	$\circ \bullet$	$\circ \bullet$	○ •	0 0			
Fill rate (β -service level)	$\circ \bullet$	$\circ \bullet$	$\circ \bullet$	$\circ \bullet$	$\circ \bullet$			
Sales targets	$\circ \bullet \bullet$	$\circ \bullet \bullet$	$\circ \bullet \bullet$	$\circ \bullet \bullet$	○ •			
Committed orders	$\circ \bullet \bullet$	$\circ \bullet \bullet$	$\circ \bullet \bullet$	$\circ \bullet \bullet$	○ •			
Net price			$\circ \bullet \bullet$	$\circ \bullet \bullet$	○ •			
Relative price to product cluster				$\circ \bullet \bullet$	○ •			
Time since last price change					○ •			
Online car configurator website traffic								
Rolling mean (windows: 3)	\circ \bullet	\circ \bullet	\circ \bullet	○ •	$\circ \bullet$			
Historic mean/standard deviation	$\circ \bullet \bullet$	$\circ \bullet \bullet$	00•	$\circ \bullet \bullet$	○ •			
Volume-weighted website traffic	\circ \bullet	0	\circ \bullet	○ •	$\circ \bullet$			
Economy and financial markets								
See Table EC.4		○ •	○ •	○ •	○ •			

Table EC.5: Data used as explanatory variables by hierarchy level. $\,$

Notes. $\circ:$ direct forecasting, $\bullet:$ hybrid forecasting, $\bullet:$ recursive forecasting

EC.6.3. Hierarchical time series

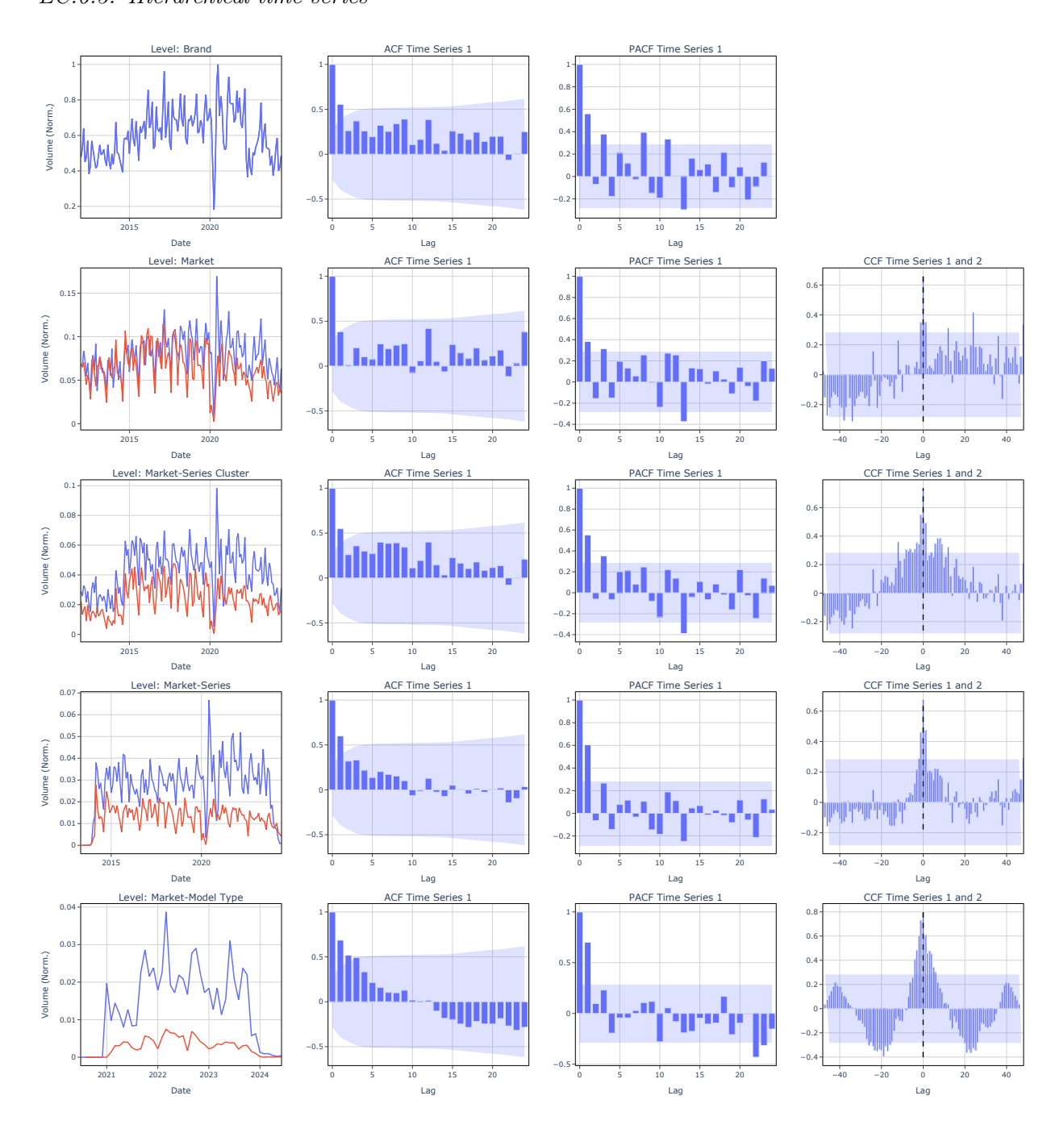


Figure EC.4: Plots of the time series, along with their ACF, PACF, and CCF.

Notes. The figure shows two example time series: series 1 (blue) and series 2 (red) across all hierarchy levels, differing only by market, not by product attributes. For each level, the autocorrelation (ACF), partial autocorrelation (PACF), and cross-correlation (CCF) are plotted. All data have been normalized for confidentiality. Visible anomalies reflect external shocks that affect forecasting accuracy, though their impact is largely mitigated in training by the length of the dataset.

EC.6.4. Hyperparameter configurations

Algorithm	Hyperparameter	Search space	Selected value
sNaive	Season length		12
MA	Window sizes		$\{2, 3, 6, 12\}$
ETS	Smoothing factor	$\{0.1,\ldots,1\}$	0.4
ARIMA	Season length		12
	Other hyperparameters for	llow Nixtla's AutoARIMA defaults.	
Prophet	Yearly seasonality		True
	Other hyperparameters for	llow the default settings of the Proph	et model as implemented by Meta.
DeepAR	Input size		12
	Objective		Quantile loss
	Iterations		1,000
	# LSTM layers	$\{1, 2, 3\}$	2
	LSTM hidden size	$\{150, \dots, 250\}$	200
	LSTM dropout rate	$\{0.01, \dots, 0.2\}$	0.1
	Decoder hidden layers	$\{1, 2, 3\}$	2
	Decoder hidden size	$\{150, \dots, 250\}$	200
	Batch size	$\{32, \dots, 128\}$	40
	Learning rate	$\{0.00001\ldots,0.1\}$	0.0001
NBEATSx	Input size		12
	MLP units		512
	Iterations		1,000
	Loss function		Quantile loss
	# Blocks	$\{1, 2, 3\}$	1
	# Harmonics	$\{2,\ldots,6\}$	5
	# Polynominals	$\{2,\ldots,6\}$	2
	Learning rate	$\{0.00001\ldots,0.1\}$	0.00609
	Activation function	{ReLU, Softplus, Tanh, Sigmoid}	Sigmoid
LightGBM	Objective (point)		Regression
	Objective (probabilistic)		Quantile
	# Estimators	$\{50, \ldots, 250\}$	153
	Max. leafs	$\{10, \ldots, 100\}$	77
	Max. depth	$\{15, \ldots, 100\}$	53
	Min. data in leaf	$\{10, \ldots, 200\}$	14
	Feature fraction	$\{0.1,\ldots,1\}$	0.952
	Bagging fraction	$\{0.1,\ldots,1\}$	0.178
	Learning rate	$\{0.001, \ldots, 0.1\}$	0.035

Table EC.6: Tuned hyperparameters selected for various forecasting models.

EC.6.5. Forecast bias

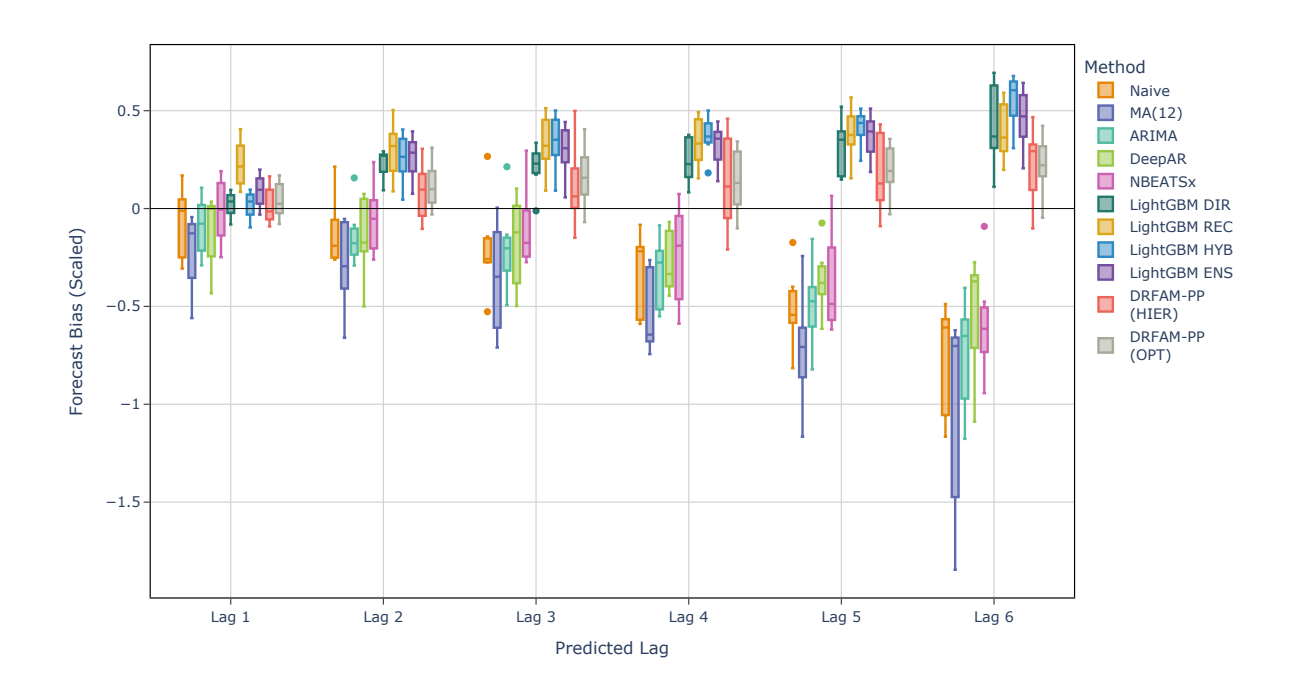


Figure EC.5: Forecast bias

EC.6.6. Scaled pinball loss

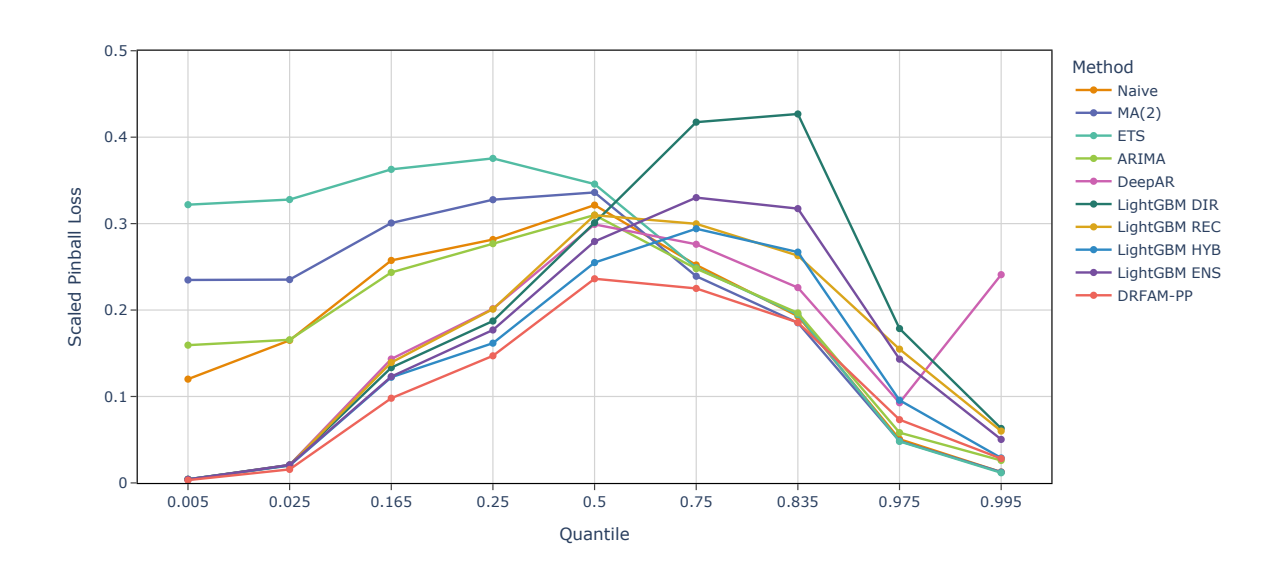


Figure EC.6: Scaled pinball loss